Deciphering magmatic processes in calc-alkaline plutons using trace element zoning in hornblende

Revision 1.

Calvin G. Barnes[1]*, Valbone Memeti[2], Nolwenn Coint[3]

[1]Department of Geosciences, Texas Tech University, Lubbock, TX 07409-1053, U.S.A.

[2]Department of Geological Sciences, California State University, Fullerton, Fullerton, CA 92834

[3]Geological Survey of Norway, PO Box 6315 Sluppen, 7491 Trondheim, Norway

*E-mail: cal.barnes@ttu.edu

ABSTRACT

Hornblende in the Kuna Crest lobe (KCL) of the Tuolumne Intrusive Complex (TIC) and the upper zone of the Wooley Creek batholith (WCB) precipitated over a temperature range of ~835 to 700°C, and thus has the potential to record magmatic processes. We measured trace element concentrations in hornblende from the WCB, from the KCL of the TIC, and from one sample from an adjacent interior unit of the TIC in order to compare and contrast magmatic processes in these two mid-crustal intrusions. In both systems the magmatic amphibole is magnesiohornblende in which Ti, Zr, Hf, Nb, Sr, Ba and rare earth elements (REE) typically decrease from crystal interiors to rims, an indication of compatible behavior of these elements, and the size of the negative Eu anomaly decreases. In the Kuna Crest lobe, hornblende from individual mapped units differs in trace element abundances and zoning trends. Some samples contain at least two distinct hornblende populations, which is particularly evident in the shapes of REE patterns. In contrast, compositions of hornblende from all structural levels of the upper WCB and related dacitic roof-zone dikes form a single broad array and the REE patterns are essentially indistinguishable, regardless of rock type, from quartz diorite to granite. In the WCB, Zr/Hf ratios in hornblende are consistent with crystallization from a melt with chondritic Zr/Hf values. In contrast, most hornblende in the KCL has Zr/Hf values lower than expected from crystallization from a melt with chondritic values, suggesting that zircon fractionation occurred before and during crystallization of the hornblende. Simple fractional crystallization models indicate that REE, high field strength elements, Sr, and Ba were compatible in KCL and WCB magmas as hornblende grew; these trends require removal of hornblende + plagioclase + zircon ± ilmenite ± biotite.

The uniform variations of trace element concentrations and patterns in the upper WCB and roof-zone dikes indicates crystallization from a large magma body that was compositionally uniform; probably stirred by convection caused by influx of mafic magmas at the base of the zone (Coint et al., 2013a, b; cf. Burgisser and Bergantz, 2011). In contrast, in the KCL, each analyzed sample displays distinct hornblende compositions and zoning patterns, some of which are bimodal. These features indicate that each analyzed sample represents a distinct magma and that individual magmas were variably modified by fractionation and mixing. Hornblende trace element contents and zoning patterns prove to be powerful tools for identification of magma

batches and for assessing magmatic processes, and thereby relating plutonic rocks to hypabyssal and volcanic equivalents.

INTRODUCTION

Results from U–Pb zircon geochronology (e.g., Mattinson, 2005; Coleman et al., 2004; Matzel et al., 2006; Michel et al., 2008; Schaltegger et al., 2009; Schoene et al., 2010; 2012; and many others) indicate that some batholith-scale magma systems are emplaced over time scales longer than thermal models predict for the longevity of individual magma batches (e.g., Tappa et al., 2011; Paterson et al., 2011). These results have led to the interpretation that large plutons are incrementally emplaced, thus raising a number of questions: (1) are individual magma batches related to one another? That is, did they form by some combination of fractional crystallization, crustal melting, magma mixing, and assimilation such that one magma batch can be related to another? (2) Regardless of petrogenesis, do magma batches interact at the level of emplacement, allowing for blending of melts and entrained crystals (e.g., Matzel et al., 2006; Miller et al., 2007; Memeti et al., 2010), or is each batch a separate intrusive entity (e.g., Coleman et al., 2004, 2012; Glazner et al., 2004)? (3) If magma batches mix, is it on a local or pluton-wide scale? The presence of large volumes of interconnected melt are seemingly required to explain homogeneous ignimbrites (Bachmann et al., 2005; Christiansen, 2005; Gelman et al., 2013), large-scale low velocity anomalies in the middle to upper crust in modern volcanic arcs (Brasse et al., 2002; Yuan et al., 2000; 2013; Ward et al., 2014), preservation of continuous hypersolidus structures in large plutons (Paterson et al., 1998; Zak et al., 2007), and the lack of observable sharp contacts that might form between individual incrementally emplaced magmas within seemingly homogeneous intrusive units (Memeti et al., 2010, but see Bartley et al., 2008, 2012). Thus, particularly in large plutons that appear to be homogeneous, it is desirable to identify a means by which individual magma batches might be identified in terms of physical, chemical, or mineralogical features. Moreover, if distinct magma batches mix, identification of components from the mixing end members is required to determine the spatial scales of mixing.

Any study of plutonic rocks must also be concerned with the relationship between bulk-rock compositions and the composition of melts from which the rocks crystallized. It may be possible to use bulk-rock compositions to identify groups of rocks that belong to a particular magma batch. However, the effects of crystal accumulation, melt percolation, and convection would obscure the identities of individual magma batches that existed. An alternative approach to using bulk rock composition as a proxy for the melt is to infer melt compositions from rock-forming minerals that reliably record the composition of the melt(s). Such records of melt composition are not affected by crystal accumulation.

This contribution is a reconnaissance of trace element compositions of hornblende from the Kuna Crest lobe (KCL) of the Tuolumne Intrusive Complex (TIC; Sierra Nevada batholith, California) and from the upper zone of the Wooley Creek batholith (WCB; Klamath Mountains, California). We chose these two systems because they are well mapped, have similar ranges of bulk composition, and have similar mineral assemblages. Our goal is to determine whether hornblende from individual intrusive units that make up large batholiths can be distinguished from one another and to learn whether intracrystalline zoning patterns can be used to interpret magmatic processes. We focus on hornblende, because it is commonly a near-liquidus phase in at least some of the magmas of interest (e.g., Piwinskii, 1973a, b; Naney, 1983, Johnson and Rutherford, 1989; Schmidt, 1992) and it incorporates many trace elements in concentrations high enough to be precisely analyzed. Mineral/melt partition coefficients have been determined for many of the trace elements of interest (e.g. Sisson, 1994; Klein et al, 1997; Brophy et al., 2011; see review in Tiepolo et al., 2007).

We find that hornblende from individual units of the KCL is distinct and that intracrystalline zoning patterns provide information about petrogenetic processes that affected individual batches. In contrast, trace element contents and zoning in hornblende from numerous samples of the upper WCB cannot be distinguished from one another, suggesting either early homogenization of the large upper zone magma (≥ 160 km^3) or virtually identical petrologic history in numerous magma batches prior to emplacement.

GEOLOGIC SETTING

Tuolumne Intrusive Complex

The Kuna Crest lobe is part of the 1,100 km^2, 95–85 Ma Tuolumne Intrusive Complex (TIC), which is exposed in the eastern Sierra Nevada batholith, central California (Fig. 1; Bateman and Chappell, 1979; Kistler and Fleck, 1994, see also Memeti et al., 2010, 2014, this volume). The TIC is one of four large composite intrusive complexes or suites emplaced near the end of the Sierran Cretaceous magma flare-up (Kistler et al., 1986; Coleman and Glazner, 1997; Ducea, 2001). The TIC is an intermediate to felsic composition, calc-alkaline, magnetite series intrusive complex that, based on Al-in-hornblende barometry, was emplaced at 8–10 km paleodepth and was not tilted after emplacement (Ague and Brimhall, 1988; Memeti et al., 2009). The complex is zoned inward and toward the northeast (Figs. 1, 2) from the oldest and most mafic units to younger and more felsic ones (Memeti et al., 2010). The most leucocratic rocks consist of the fine-grained leucocratic Johnson Granite Porphyry and small lenses within the Cathedral Peak Granodiorite (Bateman and Chappell, 1979; Kistler and Fleck, 1994; Memeti et al., 2010, 2014). Internal contacts between these units vary between sharp and gradational and commonly show zones of hybridization (Fig. 1; Žák and Paterson, 2005).

The oldest and most mafic units of the TIC are the quartz diorite of May Lake, the tonalites of Glacier Point and Grayling Lake, and the granodiorite of Kuna Crest (Bateman and Chappell, 1979; Bateman, 1992). The most extensive exposures are in a compositionally-zoned, approximately 8 by 10 km (80 km^2), body that forms the southeastern extension of the TIC that was mapped as the granodiorite of Kuna Crest (Bateman and Chappell, 1979). This unit is here referred to as the Kuna Crest lobe (KCL; Figs. 1, 2). The KCL is mostly equigranular, fine- to medium-grained granodiorite, tonalite, and diorite, although gabbroic rocks crop out in a sheeted complex along the lobe margin and elsewhere (Fig. 2; Memeti et al., this volume). Zones I, II and III are the main intrusive units of the KCL; they are separated by gradational contacts (Fig. 2; Memeti et al., 2010, this volume) and vary mainly in texture, color, and grain size. The southeastern satellite plutons around Waugh Lake and Thousand Island Lake (Fig. 2) are granodioritic to leucogranitic (Memeti et al., this volume). All Kuna Crest rocks contain anhedral to subhedral biotite and hornblende, are rich in plagioclase, and have variable amounts of alkali-feldspar (orthoclase or microcline) and quartz. The rocks contain accessory Fe-Ti oxides and zircon, and most contain titanite and allanite. Internal contacts are sharp to gradational. Magmatic fabrics tend to be strong and are locally associated with subsolidus fabrics and cm-scale shear zones (Žák et al., 2007).

Transition from the Kuna Crest lobe to the equigranular Half Dome Granodiorite (eHD) is via a hybrid zone that contains crystals typical of each unit (tHD in Fig. 2). Subhedral hornblende typical of the Kuna Crest Granodiorite occurs with larger, euhedral hornblende (≤2 cm long), euhedral biotite books (≤1 cm in diameter) and titanite (≤1 cm long) typical of the Half Dome Granodiorite (Memeti et al., 2010; this volume). The eHD in turn has gradational to sharp contacts inward to the porphyritic Half Dome Granodiorite. This unit contains hornblende and titanite similar to the eHD, but has lower color index, and contains 1–3 cm-long alkali feldspar phenocrysts. The next major unit inward is the Cathedral Peak Granodiorite (CP), which also encompasses granite and leucogranite. The modal abundances of biotite and titanite in the CP are significantly lower, hornblende is sparse, and quartz and alkali feldspar abundances are higher compared to the porphyritic Half Dome Granodiorite. Alkali feldspar megacrysts locally range to 12–15 cm in length. The Kuna Crest and Half Dome units contain abundant centimeter- to decimeter-scale mafic, microgranular, locally plagioclase-phyric enclaves, which decrease in abundance and size in pHD and are scarce to absent in the CP.

High precision CA-ID-TIMS (chemical abrasion-isotope dilution- thermal ionization mass spectrometry) U-Pb (zircon) ages reveal that crystallization of the KCL occurred at 94.9±0.3 Ma along the margin and ceased at 92.9±0.1 Ma in the Kuna Crest–Half Dome hybrid zone (Memeti et al., 2010; this volume); these ages essentially span the entire crystallization history of the Kuna Crest Granodiorite throughout the TIC. The equigranular Half Dome Granodiorite in the main TIC crystallized between 92–90 Ma, the porphyritic Half Dome Granodiorite at 90–88 Ma, and the Cathedral Peak Granodiorite at 88–85 Ma (age data summarized in Memeti et al., 2010).

Wooley Creek batholith

The Wooley Creek batholith (WCB) is a Late Jurassic pluton in the Klamath Mountains geologic province, northern California (Fig. 3). Post-emplacement tilting to the southwest followed by exhumation exposed at least 9 km of structural relief through the pluton (Barnes et al., 1986b). The pluton consists of a northeastern lower zone of biotite hornblende two-pyroxene gabbro through tonalite and a southwestern upper zone of biotite hornblende tonalite to granite (Fig. 3; Barnes, 1983; Coint et al., 2013a). Dacitic to rhyodacitic dikes (roof-zone dikes) intrude the structurally highest parts of the aureole and are interpreted to have leaked from underlying upper zone magmas. The upper zone underlies ~160 km^2 and represents a single magma body that underwent internal differentiation (Barnes et al., 1986a; Coint et al., 2013a, b). Granite and granodiorite of the upper zone are separated from the host rocks by mafic selvages in the NW and south (Fig. 3); the former is coeval and compositionally associated with the lower zone, whereas the latter is coeval with the upper zone (Coint et al., 2013a). The lower and upper zones are locally separated by the central zone, which was the site of emplacement of sheet-like bodies of upper and lower zone magmas, injection of synplutonic mafic dikes, and intense magma mixing and mingling (Coint et al., 2013a).

Emplacement ages (CA-ID-TIMS U-Pb, zircon; Coint et al., 2013a) for the lower zone are 158.99±0.17 and 159.22±0.10 Ma, for the upper zone are 158.21±0.17 and 158.25±0.46 Ma, and for the central zone are 158.30±0.16 and 159.01±0.20 Ma (all uncertainties are 2σ). Thus, although the upper and lower zones are temporally distinct, the central zone contains rocks whose ages indicate the presence of both upper and lower zone magmas. More significantly, the presence of sheets of upper-zone-like rocks in the central zone indicates growth of the upper zone reservoir by emplacement of multiple magma batches. A late-stage biotite hornblende granite, unrelated to the upper zone, was emplaced in the southern part of the batholith at 155.6±1.19 Ma (op. cit.).

Although lower-zone rocks contain magmatic hornblende, most such hornblende grew in reaction relationship with pyroxene, and in many cases inherited its trace element signature from the pyroxene (Coint et al., 2013b). Therefore, this study is focused on hornblende from the upper zone because it crystallized directly from a melt phase and because fractionation of hornblende occurred in the upper WCB magma (Barnes, 1983, 1987). The upper WCB is gradationally zoned from quartz diorite and tonalite in its eastern (lowest) part to granodiorite, quartz monzonite, and granite in its western (highest) part (Fig. 3). On the basis of Al-in-hornblende barometry (Schmidt, 1992), the transition from the central zone to the upper part of the upper zone represents 3500–5000 m of structural relief (9–14.5 km paleodepths). Mafic microgranular enclaves commonly occur in swarms in the structurally lowest part of the upper zone and, while ubiquitous, decrease in abundance upward (westward; Barnes, 1983; Coint et al., 2013a). Zonation of the upper zone was explained as the result of crystal-liquid separation via upward percolation of melt-rich magma (Coint et al, 2013a, b).

PETROGRAPHY

Kuna Crest lobe and adjacent eHD

The analyzed Kuna Crest lobe samples (petrographic descriptions in Supplemental Appendix 1) range from fine to coarse grained and are hypidiomorphic-granular tonalite and granodiorite (Fig. 4). Brown biotite and olive to green hornblende are the principal mafic minerals. Some samples contain augite rimmed by hornblende; the augite cores are variably altered to pale green amphibole ± quartz ± Fe-Ti oxides. Thus, hornblende occurs as individual prismatic grains and as rims on augite (Fig. 4A). Some hornblende is replaced by blue-green actinolitic amphibole (Fig. 4E). Sparse glomerocrysts consist of biotite ± hornblende ± relict augite ± Fe-Ti-oxides ± titanite ± plagioclase. Plagioclase is variably euhedral to anhedral and typically shows oscillatory-normal zoning (~$An_{46–33}$); some grains have rims as sodic as An_{20}. Quartz and alkali-feldspar are interstitial. If titanite is present in KCL samples, it is generally interstitial, but the sample from the hybrid unit in the interior (KCL-536, Fig. 2) contains both interstitial and prismatic (up to 0.5 cm long) titanite crystals. Other accessory minerals are apatite, magnetite ± ilmenite, zircon and rare allanite; epidote and chlorite are secondary.

Centimeter- to meter-scale porphyritic mafic enclaves with fine-grained groundmass are exposed in the hybrid granodiorite of the KCL (tHD, Fig. 2). The analyzed mafic enclave (KCL-16B) from this zone has phenocrysts of olive to green hornblende (Fig. 4D), brown biotite, and oscillatory-zoned plagioclase (~An_{35}) that reach 5 mm in length. Sparse glomerocrysts consist of hornblende ± biotite ± relict augite ± titanite ± plagioclase. The groundmass consists of stubby to elongate olive-green hornblende (Fig. 4D), brown biotite, blocky plagioclase with distinct core–rim boundaries (An_{33} & An_{20}, respectively), interstitial and poikilitic alkali feldspar, and sparse Fe-Ti oxides.

Hornblende was analyzed from one sample of the eHD adjacent to the KCL. This sample (KCL-214; Fig. 4C)) is medium- to coarse-grained granodiorite with hypidiomorphic granular texture and olive to green hornblende that occurs as euhedral crystals to one cm long, as smaller subhedral to anhedral prisms, and as interstitial grains. Some grains show patchy zoning and a few are partly replaced by blue-green actinolitic amphibole. Hornblende encloses apatite, magnetite, and plagioclase and shows minor alteration to chlorite and epidote. The remainder of the sample consists of brown, euhedral, anhedral, and subpoikilitic biotite, euhedral to anhedral plagioclase, and interstitial quartz and microcline. Some plagioclase shows broad oscillatory zoning (~An_{30}) and some has ~An_{40} cores and An_{20} rims. Euhedral titanite straddles grain boundaries (Fig. 4C), forms inclusions in microcline, and is intergrown with hornblende rims.

Wooley Creek batholith upper zone

Tonalitic to granitic rocks of the upper zone of the WCB are hypidiomorphic granular, and differ mainly in mode, with similar mineral habits among all rock types (Coint et al., 2013a). Hornblende is euhedral and seriate. Large crystals (to one cm) are zoned from patchy brown cores to green rims; some cores contain relict pyroxene. Smaller crystals are intergranular or are inclusions in quartz and alkali feldspar, and lack brown cores. Plagioclase is euhedral to subhedral, with oscillatory-normal zoning from An_{46} to An_{12} (Barnes, 1987). A weak magmatic foliation is defined by plagioclase and hornblende, whereas subhedral biotite is generally unoriented (Barnes, 1987; Coint et al., 2013a). Quartz is interstitial in tonalite and granodiorite but shows euhedral faces against interstitial to poikilitic alkali feldspar in granite. Magnetite, ilmenite, apatite, zircon, allanite, and rare anhedral tourmaline are accessory phases. Blocky prismatic zircons are present as inclusions in hornblende and plagioclase rims.

Roof dikes related to the upper zone range from andesite to rhyodacite in composition. These dikes contain up to 55 percent phenocrysts of hornblende and plagioclase ± quartz ± augite ± biotite. Groundmass textures range from fine equigranular to granophyric.

METHODS

Hornblende and plagioclase major element concentrations reported here were determined by electron microprobe (EMP) at the Univ. of California-Los Angeles or the Univ. of Oklahoma. Typical operating conditions were 20 kV accelerating voltage, 20 nA beam current, and 1–2 µm spot size, using natural and synthetic standards. Data and analytical methods for hornblende from the WCB are reported in Barnes (1987) and Coint et al. (2013b).

Trace element abundances were collected in situ, in polished sections, by laser ablation inductively-coupled plasma mass spectrometry (LA-ICP-MS) analysis using a NewWave 213 nm solid-state laser and Agilent 7500CS ICP-MS at Texas Tech University. Operating conditions were spot diameter 40 μm, laser pulse rate of 5 Hz, and fluence of 11–12 J cm^{-2}. For each analysis, 25s of background (laser off) and 60s of signal were recorded. The analytical standard was NIST 612 glass; it was analyzed after every 5–7 unknown analyses. Precision was determined by repeated analysis of basaltic glass BHVO-2g and ranges from 2.5–12% (relative; Coint et al., 2013b). Trace element abundances were normalized to abundances of CaO or SiO_2, as determined by electron microprobe; no statistical difference between normalization with CaO or SiO_2 contents was found.

Wherever possible, laser ablation spots were located on or adjacent to EMP analytical spots (see Table 2 for representative data and Supplemental Table 1 for the complete data set and analytical details). Comparison of MnO and TiO_2 concentrations determined by EMP and laser ablation (Supplemental Table 1) shows good correlation for both elements, although Ti shows greater scatter than Mn. This scatter is ascribed to the differences in analytical volume between the two methods: ca. 10 μ^3 for EMP versus ca. 35 x 10^5 μ^3 for laser ablation analysis. The former method is prone to error due to fine-scale features such as thin ilmenite lamellae, whereas the latter method is prone to error due to intersection of inclusions such as apatite, Fe-Ti oxides, and zircon. All laser ablation spectra and reduced data were inspected for anomalous quantities of P, Ti, and Zr and analyses with such anomalies were omitted from the data set.

BULK-ROCK COMPOSITIONS OF THE KCL AND WCB

Direct comparison of hornblende compositions from the KCL and WCB supposes that the hornblendes crystallized from similar melts at similar temperatures. Here, we use a plot of CaO versus Sr contents (Fig. 5) for comparison of bulk-rock compositions (data from Coint et al., 2013a; Bateman and Chappell, 1979; Burgess & Miller, 2008; Gray et al., 2008; and Memeti et al., this volume and Table 1). The upper zone of the WCB and the KCL overlap in terms of CaO content (Fig. 5) but nearly all Kuna Crest samples have higher Sr contents than the WCB upper zone samples. For other elements of interest, concentrations for the KCL and WCB are, respectively: TiO_2, 0.7–1.1 and 0.1–1.0 wt%; Ba, 400–1300 and 410–890 ppm; Nb, 4.5–10 and 3.5–9.5 ppm; Zr, 86–272 and 65–190 ppm; Hf, 3–6 and 2–4 ppm.

RESULTS

Hornblende compositions

The amphiboles are calcic and plot in the magnesiohornblende field (Fig. 6A). Amphibole structural formulas (Esawi, 2004) were calculated with all Ca in the M4 site; nearly all such calculations resulted in stoichiometric formulas (Leake et al., 1997). Hornblende from the KCL and eHD has a narrow range of $Mg/(Mg+Fe^{2+})$ from 0.62 to 0.77, and the $Mg/(Mg+Fe^{2+})$ value increases with increasing Si (Fig. 5A). In contrast, twelve samples from WCB upper zone and roof-zone dikes and ten mafic magmatic enclaves show a wide range of $Mg/(Mg+Fe^{2+})$, although individual samples plot in narrow arrays parallel to those of KCL hornblende. Most WCB samples have lower $Mg/(Mg+Fe^{2+})$ than TIC hornblende (Fig. 6A). One exception is sample MMB-379, which was collected in a zone with numerous swarms of mafic enclaves.

Titanium contents show a regular negative correlation with Si for all samples (Fig. 6B). In samples with prismatic hornblende, intra-crystal zoning is from Ti-richer cores to Ti-poor rims. The Al contents of hornblende also decrease with increasing Si (Fig. 6C). Variation of Na broadly correlates with Ti (not shown). As with Al, the highest Na contents are seen in cores of hornblende phenocrysts in the mafic enclave (KCL-16B) and in hornblende from the southern tip of the KCL.

Inasmuch as magmatic systems such as the TIC have been proposed as the plutonic analogues of giant, monotonous dacitic ignimbrites (e.g., Gelman et al., 2014; Graeter et al., 2015; Lipman and Bachmann, 2015), hornblende compositions from the ca. 5000 km^3 Fish Canyon Tuff (Bachmann and Dungan, 2002) are shown for comparison in Figure 6. Hornblende from the Fish Canyon Tuff is more magnesian than most WCB and all KCL hornblende, but is similar to both in terms of Ti and Al contents.

Temperatures of hornblende crystallization were calculated using a pressure-independent thermometer based on concentrations of Si, Ti, Fe, and Na, in which the calibration data are reproduced to ±29°C (Putirka, in review). Temperature (T) calculated for olive-green KCL hornblende range from 836 to 722°C, except for sample KCL-536A from the KCL–eHD hybrid zone, in which some rim temperatures are as low as 708°C. Olive-green hornblende from eHD sample KCL-214 yielded an average T of 741±16°C. In contrast, temperatures calculated for blue-green amphibole that locally rims and replaces olive-green hornblende range from 707–686°C, indicating that the blue-green amphibole is probably near-solidus or sub-solidus replacement of magmatic olive-green hornblende. Olive-green hornblende from the upper WCB and roof-zone dikes yields temperatures in the range of 824–702°C. A single exception is roof-zone dike MMB-579, which contains pale green hornblende that yields temperature estimates from 690–666°C.

Trace element abundances generally vary as a function of Ti contents. For example, hornblende from the WCB upper zone broadly decreases in Sr and Nb with decreasing Ti (Fig. 7A, B), with broad overlap in compositions from one sample to the next. In contrast, hornblende compositions of individual samples from the KCL and from eHD sample KCL-214 tend to plot in sub-parallel but distinct compositional arrays (Fig. 7A–D). One exception to these parallel trends is the behavior of Nb and Ta in sample VLM-2 from the southern tip of the KCL (Fig. 2). In this sample, hornblende increases in Nb and Ta from core to rim (Fig. 7B, D).

Hornblende from the upper zone of the WCB has Zr/Hf ratios of ~20:1, whereas KCL hornblende compositions plot in arrays with shallower slopes (Fig. 7C). Similarly, hornblende from the upper WCB has a range of Ta/Nb ratios of ~0.03 to ~0.08 and samples from the KCL have a somewhat wider range of values (0.01–0.09; Fig. 7D). Barium concentrations in WCB upper zone hornblende vary by more than 220 ppm for the entire unit and by as much as 160 ppm among individual samples (Fig. 7F); Ba decreases with decreasing Ti content. Only two KCL samples (mafic enclave KCL-16B and VLM-2 from the southern Waugh Lake pluton) have hornblende with Ba contents as high as seen in WCB hornblende, with the remainder of the KCL hornblende having less than 35 ppm Ba (Fig. 7F).

Among the transition metals, Sc shows weak or no correlation with Ti and V decreases slightly with decreasing Ti (not shown). Chromium contents in WCB upper-zone hornblende range from ~50 to ~400 ppm but are <50 ppm in KCL hornblende. No correlation between Cr and Ti was observed in either suite. However, in the mafic enclave from the KCL (sample KCL-16B), hornblende phenocrysts have < 50 ppm Cr, in the same range as other KCL samples, but groundmass hornblende contains 63–247 ppm Cr. The Cr-poor phenocrysts are also distinct in having higher Ti and Nb than the groundmass hornblende (Fig. 7B).

The REE patterns of hornblende from the upper WCB (Fig. 8A) and dacitic/rhyodacitic roof-zone dikes are very similar to one another (Coint et al., 2013b). In any given sample, the REE abundances typically show a 3-fold variation in abundance, with most crystals zoned from REE-richer cores that have moderate negative Eu anomalies to REE-poorer rims with smaller Eu anomalies (Coint et al., 2013b).

In contrast to the uniformity of hornblende REE compositions in the WCB, hornblende from the KCL samples varies widely in REE abundances and patterns (Fig. 8). This diversity includes REE compositions of deuteric, actinolitic amphibole, with REE abundances < 10 times chondrites and essentially flat patterns. These patterns are omitted from Figure 8 for the sake of clarity.

Among the KCL samples, hornblende from the outer unit (zone I; Fig. 2) has the highest REE abundances and displays the deepest negative Eu anomalies (Fig. 8A). Hornblende from KCL zone III (Fig. 2) has lower total REE abundances and steeper slopes than zone I hornblende (Fig. 8B). Most zone III hornblende grains are zoned from higher total REE in the cores to lower total REE in the rims. In both zone I and zone III samples, the slope of the heavy REE is negative from Gd to Lu (Fig. 8A, B). The sample from the hybrid zone between the KCL and the eHD (KCL-536A; unit tHD in Fig. 2) shows the greatest diversity of REE patterns (Fig. 8C). The majority of analyzed hornblende in this sample has light and middle REE abundances slightly lower than hornblende from KCL unit III. However, in these samples the heavy REE patterns show a concave shape unlike the patterns in hornblende from KCL units I and III (Fig. 6C). Rim compositions have significantly lower REE abundances than crystal interiors, smaller Eu anomalies, and more pronounced concave shape. One analyzed hornblende grain (crystal 16B; Fig. 8C) has considerably lower REE abundances compared to the other crystals but shares the concave shape in the heavy REE that characterizes the other hornblende grains. Lastly, a hornblende inclusion in a plagioclase phenocryst has a REE pattern whose shape is similar to that of hornblende from KCL unit I and lacks upward concavity in the heavy REE, but has much lower REE abundances than KCL unit I hornblende.

Rare earth element abundances in hornblende from the KCL lobe tip (VLM-2; Waugh Lake pluton) decrease from interior to rim and the heavy REE patterns develop a concave shape toward crystal rims (Fig. 8D). Phenocrysts in the mafic enclave (KCL-16B; Fig. 8E) have REE patterns similar to hornblende in KCL zone III, whereas groundmass hornblende has lower REE abundances, slightly steeper slopes, and less pronounced Eu anomalies. Hornblende from the equigranular Half Dome sample (Fig. 8F) is similar in shape to hornblende from the KCL lobe, but with lower total REE abundances and slight concave shape in the heavy REE.

DISCUSSION

One of the goals of this study is to compare the variations within and differences among hornblende in WCB and TIC samples and to use observed variations to determine whether trace element abundances in hornblende could be used to identify magma batches. We presume that intra-crystalline abundances and variation of trace elements in magmatic amphibole varied as a function of changes in melt composition. This premise is supported by the presence of zoning in the amphibole and by the fact that the mafic enclave (KCL-16B) contains two petrographically and geochemically distinct populations of hornblende: large crystals with relatively higher contents of Ti, Nb, and the REE, and lower Cr, and fine-grained groundmass hornblende with lower Ti, Nb, and REE and higher Cr (Figs. 7 and 8). If diffusion were able to homogenize hornblende at the scale of hand samples, we would expect homogenization of crystal compositions in this sample, particularly of the fine-grained hornblende. Also, rapidly-diffusing elements such as Sr and Ba co-vary with slow-diffusing HFSE in each of the analyzed samples, indicating that intra-crystalline diffusion and/or exchange with adjacent phases did not strongly affect the magmatic trace element signature.

Magma mixing

The zone from which sample KCL-536A was collected is interpreted to be a hybrid between KCL and eHD magmas on the basis of broad gradational contacts between KCL- and eHD-like rock units, habits of hornblende and biotite characteristic of both units, and whole-rock initial ratios of Sr and Nd isotopes transitional between the two units (Memeti et al., 2010, this volume). Compositions of crystal interiors in this sample identify two populations, one formed by four different analyzed grains and the other by a single analyzed grain, crystal 16B (Fig. 8C). In addition, the hornblende inclusion in plagioclase evidently represents a third hornblende population, with a distinctive REE pattern (Fig. 8C). These distinct hornblende populations are consistent with sample KCL-536A being a hybrid of KCL and eHD magmas.

If sample KCL-536A is a hybrid of KCL lobe magma with eHD magma, then it is noteworthy that hornblende from the single analyzed sample of the eHD (KCL-214A) is distinct from any hornblende in KCL-536A in having lower Sr and higher Nb at a given Ti content (Fig. 7A, B). This discrepancy may point to the possibility that hornblende in the eHD is not homogeneous but varies from one sample to the next—a testable hypothesis. Alternatively, it is possible that multiple populations of hornblende can be evaluated in the same way as zircon, in the sense that some crystals grew from their host melt (autocrysts), whereas others grew from older magmatic units (antecrysts; cf. Miller et al., 2007; Memeti et al., 2014).

The bimodality of both crystal size and composition in enclave sample KCL-16B (Fig. 7, 8E) is also consistent with a hybrid origin. In this case, we interpret the large hornblende (and plagioclase and biotite) crystals to be derived from a relatively evolved, porphyritic magma. The groundmass hornblende, with relatively high Cr and low REE contents, crystallized from a hybrid melt formed by mixing of the evolved, phenocryst-bearing magma with a less evolved magma.

Hornblende from the Waugh Lake pluton in the southern tip of the KCL tip (VLM-2; Fig. 2) is distinct in having higher Nb and Ta concentrations in crystal rims than interiors, with a distinct compositional gap between them (Fig. 7D). These hornblendes also have the highest Ba and Zr concentrations of any KCL sample; however, both Ba and Zr decrease from core-to-rim (Fig. 7C, F). It is possible that the increases in Nb and Ta concentrations result from fractional crystallization in which both Nb and Ta were incompatible—despite the fact that both elements are compatible in all other samples. However, fractional crystallization does not explain the distinct gap in, for example, Nb concentrations from < 25 ppm in cores to >30 ppm in rims (Fig. 7D). The rim compositions could also be explained if a phase rich in Nb and Ta (e.g., titanite) were resorbed during growth of hornblende rims. This explanation is problematic because interstitial titanite in this sample occurs late in the crystallization sequence. Alternatively, the Nb- and Ta-rich rims could have formed as the result of magma mixing in which the recharge magma was relatively enriched in both elements. It is noteworthy that at least with regard to Nb, Ta, Ti, and Ba, rim compositions of VLM-2 hornblendes are similar to those of hornblende from unit KCL I (Fig. 7).

Fractional crystallization

In a detailed study of another lobe of the TIC, the southern Half Dome lobe (Fig. 1), whole-rock element and isotope data were used to interpret magma differentiation by fractional crystallization (Economos et al., 2010). In contrast, cross-cutting relationships and geochronologic data from the KCL indicate that magmas intruded and crystallized over ca. 2 my (Fig. 2; Memeti et al., 2010; this volume). These data argue against formation of a lobe-wide melt-interconnected KCL magma chamber. However, the similarities in whole-rock Sr and Nd initial isotope ratios (Memeti et al., this volume) are permissive of deep-crustal evolution of KCL magmas by fractional crystallization. This possibility can now be evaluated using hornblende trace element trends (Fig. 7) and REE patterns (Fig. 8).

A simple approach to assessing fractional crystallization is to model intra-crystalline and intra-sample trace element variation within hornblende as a proxy for melt evolution. The trace element composition of melt in equilibrium with hornblende can be calculated from the partition coefficient ($k = c_{min}/c_{melt}$, where c = concentration in ppm). In addition, the degree of crystallization (F = mass fraction of melt remaining) can be constrained by the Rayleigh fractionation equation, commonly expressed as the concentration ratio of the daughter liquid to the parent liquid, $c_{melt}/c_o = F^{(D-1)}$ (Greenland, 1970),where D is the bulk partition coefficient. If k is constant, then the Rayleigh fractionation equation can be recast in terms of mineral compositions: $c_{melt}/c_o = c_{min}/c_{min,o} = F^{(D-1)}$, where $c_{min,o}$ = trace element concentration in the mineral core.

Variation of Zr, Hf, Ta, and Nb in hornblende from two KCL samples and one WCB sample were calculated using the approach described above (Fig. 7C, D, E). All of these elements are assumed to be compatible in the magmatic system, because their abundances decrease from crystal interiors to rims. Bulk partition coefficient values between 1.8 and 2.5 fit the data and yield estimates of the fraction of melt remaining (F) from 1 to ~ 0.7 for the two modeled KCL samples and 1 to ~0.45 for the upper WCB sample (Fig. 7C, D, E). These models are simplistic in terms of the assumption of constant D values, because D is expected to increase with decreasing temperature. However, the linearity of element trends indicates that even if D values increased with decreasing temperature, they must have varied sympathetically to maintain the linear trends. In addition, if D increases during differentiation, then estimates of F based on constant D values represent maximum values.

The calculations are consistent with fractional crystallization as the cause of intra-sample variation of trace elements in each sample. The calculations also illustrate the difficulty in producing KCL III-type magma from KCL I-type magma by fractional crystallization. This relationship in turn suggests that if any direct petrogenetic relationship between KCL I-type and KCL III-type magmas existed, it must have involved deep-seated magma mixing in order to reset hornblende core compositions back to higher concentrations of compatible elements.

The compatible behavior of Sr, Ti, and Ba in KCL and WCB hornblendes suggests fractionation of hornblende along with plagioclase, Fe-Ti oxides, and biotite. The striking decrease in Ba contents in upper WCB hornblende (e.g., Fig. 7F) compared to the minor decreases in KCL I and KCL III hornblende (Fig. 7F) cannot be explained by alkali feldspar or plagioclase fractionation, because alkali feldspar is sparse in many WCB samples and interstitial in all of them (Coint et al., 2013b), and because Ba is mildly incompatible in WCB plagioclase (<300 ppm in plagioclase, >350 ppm in bulk-rocks; Barnes, unpublished data). In contrast, biotite from the upper zone contains ~5000 ppm Ba (Barnes, unpublished data), such that biotite fractionation would result in compatible behavior of Ba.

Partition coefficients for the REE and HFSE between hornblende and melt vary significantly (e.g., Bachmann et al., 2005; Tiepolo et al., 2007). Partition coefficients for the REE in hornblende crystallized in evolved melts at the relatively low temperatures measured for KCL and WCB hornblende are likely to be > 1, and significantly higher for the heavy REE (Bachmann et al., 2005). Thus, fractionation of hornblende with high k_{REE} values can explain the rim-ward decrease in REE (e.g., Coint, 2013b). However, with the possible exception of Nb (Tiepolo et al., 2007; Tiepolo and Vannucci, 2014), hornblende fractionation is unlikely to be responsible for compatible behavior of the HFSE. The compatible behavior of Zr and Hf is probably due to fractionation of zircon, and although Nb is likely to be weakly compatible in hornblende, the highest partition coefficient for Ta in hornblende reported by Tiepolo et al. (2007) is 1.0. Thus, in addition to hornblende, biotite ± ilmenite fractionation is likely to be responsible for the decreases in Nb and Ta (e.g., Bea et al., 1994; Stepanov and Hermann, 2013). It is noteworthy that fractionation of titanite cannot explain the Nb and Ta decrease in upper WCB samples, because magmatic titanite is absent. Similarly, magmatic titanite is sparse in the KCL I and KCL III samples; thus decreases in Nb and Ta are thought to be caused by biotite fractionation.

Petrogenetic relationships between KCL units

The compositional variations in the KCL as recorded at the whole rock (Memeti et al., this volume) and the mineral scales (this study), are not consistent with the lobe-wide fractionation model applied to the southern Half Dome lobe (Economos et al., 2010). The compositional arrays of hornblende from zones I and III of the KCL indicate that melts in each magma unit were fractionated by removal of hornblende and other phases, and that this fractionation could have occurred in situ. However, differentiation of KCL magmas solely by

This is a preprint, the final version is subject to change, of the American Mineralogist (MSA)
Cite as Authors (Year) Title. American Mineralogist, in press.
(DOI will not work until issue is live.) DOI: http://dx.doi.org/10.2138/am-2016-5383 10/7

fractional crystallization at the level of emplacement is highly unlikely given that individual samples do not lie along a single compositional array. Instead, Figures 7 and 8 show that hornblende from each sample is distinct and in many cases has trace element variation that is neither collinear with, nor parallel to trends of other samples. It is possible that the KCL represents a magma conduit and therefore reflects changing magma compositions in a deeper reservoir. Nevertheless, we find it extremely difficult to explain the differences in hornblende trace element arrays (Fig. 7) and REE patterns (Fig. 8), or variation in the whole-rock data (Memeti et al., this volume), in terms of differentiation in a deep crustal reservoir without episodic influx of numerous, compositionally diverse magmas. Evaluation of such processes will require detailed characterization of hornblende from numerous samples, including detailed analysis of hornblendes from individual mapped intrusive units. At this stage of the research on KCL hornblende, some general observations can be made.

(1) The Zr/Hf ratio of hornblende varies from one sample to the next and all of the KCL hornblendes have Zr/Hf ratios lower than expected if the hornblende crystallized in magmas with chondritic values (Bea et al., 2006), with the lowest ratios in hornblende from the equigranular Half Dome sample (Fig. 7C). These ratios are in contrast to hornblende in the upper WCB, which plot on either side of the value expected from crystallization from a chondritic melt (Fig. 7C). Among the phases stable in TIC magmas, zircon is the only one capable of significantly lowering Zr/Hf because of its high Zr/Hf ratio (~47; Bea et al., 2006; Claiborne et al., 2006, 2010; Colombini et al., 2011) and high concentrations of both elements. Fractionation of titanite would have the opposite effect of zircon, because the Zr/Hf ratio of titanite ranges from 10–20. The fact that the Zr/Hf ratio in hornblende, an early-crystallizing phase in the KCL, varies from sample to sample suggests that zircon fractionation occurred in the magma source and/or storage

zones. This conclusion is consistent with saturation of zircon in KCL magmas, as indicated by the presence of antecrystic zircon (Coleman et al., 2004; Miller et al., 2007; Burgess and Miller, 2008; Memeti et al., 2010, 2014) and locally with xenocrystic zircon in the KCL (Memeti et al., this volume).

(2) Trace element data for hornblende from the interior hybrid zone of the KCL (sample KCL-536A) are consistent with in-situ mixing of KCL magma with eHD magma. However, hornblende compositions in sample KCL-536A are distinct from those of other samples of the KCL, and they are also distinct from the hornblende in our single analyzed sample from the eHD (e.g., Figs. 7, 8). Questions therefore remain: Are hornblende compositions and zoning patterns uniform within the main units of the TIC, or do these units carry heterogeneous hornblende cargos that contain autocrystic and antecrystic hornblende, ± hornblende inherited from magma mixing events? The mafic enclave from the central hybrid unit is clearly a mixture in which neither the phenocrysts nor the groundmass crystals can be directly related to other KCL hornblendes. In this instance, the data indicate that the enclave magma was hybridized prior to transport to the level of intrusion.

(3) The relatively low abundances of Sr and Ba in most KCL samples (compared to WCB hornblende) indicate that hornblende in most TIC samples grew from Sr- and Ba-depleted melts. Low Sr abundances can be explained by sequestration in plagioclase, which would also explain the prominent negative Eu anomalies in hornblende REE patterns. Although Ba is readily accepted in alkali feldspar, KCL samples lack alkali feldspar phenocrysts that characterize the pHD and CP units. Instead, the alkali feldspar is poikilitic and interstitial, indicating late growth in KCL magmas. Moreover, the Ba contents in plagioclase are low (~220 ppm; Supplemental Table 2) compared to bulk-rock values (546–1143 ppm; Table 1), thus, the compatible behavior

of Ba is presumably due to fractionation of biotite.

Calculated melt compositions

The simple fractional crystallization models discussed above permit calculation of trace element concentrations in the equilibrium melt if appropriate mineral/melt partition coefficients are available. Partition coefficients published by Klein et al. (1997) and Bachmann et al. (2005) were used in these calculations. In Table 3, calculated melt compositions are compared to measured bulk-rock compositions (data from Coint et al., 2013a for the upper WCB and Table 1 for the KCL). For the KCL zone III sample (KCL-390), Ba, Sr, Zr, and Hf have higher bulk-rock concentrations than were calculated for melt in equilibrium with hornblende, whereas Nb, Ta, and Ce have lower bulk-rock concentrations. If the k values used to calculate melt compositions are appropriate, then results of the calculations suggest that the sample is a partial cumulate of plagioclase + zircon ± biotite and that the lower abundances of Nb, Ta, and Ce indicate dilution by accumulation of phases such as plagioclase, along with the absence of cumulate allanite or titanite. In contrast, calculated melts in equilibrium with hornblende in the upper WCB sample have higher abundances of all modeled trace elements except Sr, which suggests that the rock contains cumulate plagioclase (Barnes et al., 2013). It is premature to place too much importance on calculated melt compositions in light of uncertainties in magmatic temperatures and the range of published k values for these elements (Tiepolo et al., 2007). However, as data for partition coefficients improve, particularly for low-T magmatic systems, it will be possible to critically assess the importance of crystal accumulation on trace element contents of plutonic rocks.

Implication for study of incrementally emplaced magma batches

Some incremental emplacement models of pluton growth call on emplacement of small magma batches which do not mix appreciably with pre-existing magma batches at the emplacement level (Glazner and Bartley, 2006; Bartley et al., 2008), thus limiting opportunities for producing large, homogeneous magma bodies. Eruptions of medium- to large-volume ignimbrites provide clear evidence for, at the very least, ephemeral, large-volume magma bodies, many of which are compositionally zoned. The question is whether evidence of such 'eruptible' magma bodies is preserved in the plutonic record.

The consistency of the hornblende trace element abundances in the upper WCB is remarkable compared to the diversity seen in the KCL, particularly in view of the exposed area of the upper WCB: ~160 km^2. Although it is possible that percolation of melt along with intracrystalline diffusion in the upper zone of the WCB during slow cooling could homogenize hornblende trace element compositions (e.g., Boudreau, 2011), the fact that intracrystalline zoning is preserved and repeated from hornblende in tonalite to granite over the entire area of the upper zone argues against pluton-scale homogenization by diffusive processes. Coint et al. (2013b) interpreted the widespread consistency of hornblende REE patterns and abundances in the upper WCB to indicate that hornblende crystallized from a single, differentiating magma batch. Although it is possible that the upper zone crystallized from multiple magma batches with remarkably similar bulk compositions, and that the internal intrusive contacts were obscured (Glazner et al., 2004; Bartley et al., 2008), the fact that distinct batches cannot be found in the upper (cooler) zone of the batholith, but are well preserved in the lower (hotter) zone, argues against such an interpretation. In addition, if the upper zone formed from discrete batches that did not mix, then the bulk-rock compositional variation in the upper zone from structurally lower tonalite to structurally higher granite, all with identical U-Pb ages, would be highly fortuitous.

The KCL hornblende is like WCB upper zone hornblende in having similar major element compositions; however, not only are the trace element concentrations of KCL hornblendes distinct from one unit to the next, but they also show considerably greater compositional diversity than hornblende from the upper WCB. Thus, even if we lacked the clear field evidence for incremental emplacement of the KCL (Memeti et al., this volume) and the U-Pb (zircon) ages indicating prolonged emplacement, the trace element compositions and trends in KCL hornblende would make it possible to detect multiple magmatic units, each of which appears to have a distinct petrogenetic history. Because of the reconnaissance nature of our sampling, it remains to be seen whether hornblende *within* specific units of the KCL differs from one sample to the next. Answers to this question will help determine whether the mapped subunits of the KCL represent singular, relatively large magma batches (for example, at the scale of a mapable KCL unit) or an accumulation of smaller, sub-unit-sized magma batches.

IMPLICATIONS

Trace element variation in rock forming minerals provides an excellent but rarely used tool to study the assembly of calc-alkaline plutons, to identify and model magmatic processes responsible for compositional variation of individual magma units, and to place constraints on the spatial extent of, and chemical connectivity within, magma bodies. In examples of uniform trace element variation, such as the upper WCB and roof-zone dikes, the similarities in major and trace element concentrations and patterns of hornblende over a range of rock types and SiO_2 contents can provide evidence for large reservoirs of crystal-rich magma with interconnected melt, and the dikes attest to the fact that this magma body was ‘eruptible’ during part of its history (Coint et al., 2013a, b). In contrast, in plutonic units such as the Kuna Crest lobe, trace element data on hornblende can provide evidence for the presence of distinct, diachronous magmatic units. Mixing of distinct magmas can also be distinguished, as for example in the KCL interior hybrid zone. This study shows the potential for identification of pervasive mixing; however, much more detailed data will be required to assess mixing on a pluton-wide scale. Hornblende zoning patterns may also show clear evidence for fractional crystallization, either at the scale of hand specimens or of individual magmatic units.

In some instances, the calculated concentrations of trace elements in the *melts* in equilibrium with hornblende are quite distinct from bulk-rock compositions. These distinctions may be used to identify rocks that are cumulates and comparisons of calculated melt versus bulk-rock compositions will indicate which minerals have accumulated. Our data suggest that the bulk-rock compositions of calc-alkaline plutonic rocks should be used cautiously to interpret melt compositions and liquid lines of descent.

Our results indicate that hornblende in the KCL preserves evidence for magma mixing, both in situ and below the level of emplacement. In each example of mixing, the end member compositions are as diverse as the various intrusive units exposed in the lobe. The implication of this variety of compositions is that a potentially large variety of similar, but distinct, magmas assembled prior to and during emplacement of the Kuna Crest stage of the TIC. These distinctions, discernable from hornblende compositions, may not be recognized from bulk-rock data.

The uniform, Zr/Hf ratio in WCB hornblendes is distinct from the lower values in most KCL hornblendes. The lower Zr/Hf ratios in KCL hornblende suggest that zircon fractionated from the parental melts. The interpretation that this fractionation began in the source region and may have continued during transport and at the level of emplacement has important implications for the origins and fate of xenocrystic and antecrystic zircon in similar plutons. It is possible that detailed traverses on many grains from single samples could identify the onset of zircon fractionation.

When coupled with field, textural, bulk-rock geochemical, and geochronologic study, trace element compositions of hornblende provide a powerful tool for tracing changes in melt compositions in plutonic rocks. Such data can be used to assess magma differentiation processes, the pace of magma emplacement, size of magma batches and volumes of melt-interconnected magma mush, and thus the size of magma reservoirs.

ACKNOWLEDGEMENTS

We thank Danielle Olinger and Melanie Barnes for their work on laser ablation analyses of TIC samples. Memeti is grateful for the continued logistical support from the park rangers at Yosemite National Park and park geologist Greg Stock. We thank Anita Grunder, Tom Sisson, and Calvin Miller for helpful, thought-provoking reviews and Scott Paterson and Aaron Yoshinobu for comments on early versions. Research on the Wooley Creek batholith was supported by NSF grant EAR-0838342 (A.S. Yoshinobu & Barnes) and a Geological Society of America Penrose grant to Coint. Memeti was supported by NSF grant EAR- 0440073 for her initial work on the TIC as a graduate student at the Univ. of Southern California. Memeti also thanks the geologic mapping education component of the U.S. Geological Survey National Cooperative Geologic Mapping Program (EDMAP) for three consecutive years for mapping the TIC lobes.

REFERENCES CITED

Ague, J.J., and Brimhall, G.H. (1988) Regional variations in bulk chemistry, mineralogy, and the compositions of mafic and accessory minerals in the batholiths of California. Geological Society of America Bulletin, 100, 912–927.

Bachmann, O., and Dungan, M.A. (2002) Temperature-induced Al-zoning in hornblendes of the Fish Canyon magma, Colorado. American Mineralogist, 87, 1062–1076.

Bachmann, O., Dungan, M. A. and Bussy, F. (2005) Insights into shallow magmatic processes in large silicic magma bodies: the trace element record in the Fish Canyon magma body, Colorado. Contributions to Mineralogy and Petrology, 149, 338–349.

Barnes, C.G. (1983) Petrology and upward zonation of the Wooley Creek batholith, Klamath Mountains, California. Journal of Petrology, 24, 495–537.

Barnes, C.G. (1987) Mineralogy of the Wooley Creek batholith, Slinkard pluton, and related dikes, Klamath Mountains, northern California. American Mineralogist, 72, 879–901.

Barnes, C.G., Allen, C.M., and Brigham, R.H. (1987) Isotopic heterogeneity in a tilted plutonic system, Klamaht Mountains, California. Geology, 15, 523–527.

Barnes, C.G., Allen, C.M., and Saleeby, J.B. (1986a) Open- and closed-system characteristics od a tilted plutonic system, Klamath Mountains, California. Journal of Geophysical Research, 91, 6073–6090.

Barnes, C.G., Rice, J.M., and Gribble, R.F. (1986b) Tilted plutons in the Klamath Mountains of California and Oregon. Journal of Geophysical Research, v. 91, p. 6059-6071.

Barnes, C.G., Coint, N., and Memeti, V. (2013) Use of trace element zoning in hornblende to identify magma batches and reservoirs and decipher magmatic processes in calc-alkaline plutons. Geological Society of America Abstracts with Programs, 45, 230.

Bartley, J.M., Coleman, D.S., and Glazner, A.F. (2008) Incremental pluton emplacement by magmatic crack-seal. Transactions of the Royal Society of Edinburgh: Earth Sciences, 97, 383–396.

Bartley, J.M., Glazner, A.F., and Mahan, K.H. (2012) Formation of pluton roofs, floors, and walls by crack opening at Split Mountain, Sierra Nevada, California. Geosphere, 8, 1086–1103.

Bateman, P.C. (1992) Plutonism in the central part of the Sierra Nevada Batholith, California. U.S. Geological Survey Professional Paper, 1483, 1-186.

Bateman, P.C., and Chappell, B.W. (1979) Crystallization, fractionation, and solidification of the Tuolumne intrusive series, Yosemite National Park, California. Geological Society of America Bulletin, 90, 465–482.

Bea, F., Pereira, M.D. and Stroh, A. (1994). Mineral/leucosome trace-element partitioning in a peraluminous migmatite (a laser ablation-ICP-MS study). Chemical Geology, 117, 291–312.

Bea, F., Montero, P., and Ortega, M. (2006) A LA-ICPMS evaluation of Zr reservoirs in common crustal rocks: Implications for zircon-forming processes. The Canadian Mineralogist, 44, 693–714.

Boudreau, A., (2011) The evolution of texture and layering in layered intrusions. International Geology Review, 53, 330–353.

Brasse, H., Lezaeta, P., Rath, V., Schwalenberg, K., Soyer, W., and Haak, V. (2002) The Bolivian Altiplano conductivity anomaly. Journal of Geophysical Research, 107, doi:10.1029/2001JB000391

Brophy, J.G., Ota, T., Kunihiro, T., Tsujimori, T., and Nakamura, E. (2011) In situ ion-microprobe determination of trace element partition coefficients for hornblende, plagioclase, orthopyroxene, and apatite in equilibrium with natural rhyolitic glass, Little Glass Mountain Rhyolite, California. American Mineralogist, 96, 1838–1850.

Burgess, S.D., and Miller, J.S. (2008) Construction, solidification and internal differentiation of a large felsic arc pluton: Cathedral Peak granodiorite, Sierra Nevada Batholith. Geological Society, London, Special Publication, 304, 203–233. doi:10.1144/SP304.11.

Burgisser, A., and Bergantz, G.W. (2011) A rapid mechanism to remobilize and homogenize highly crystalline magma bodies. Nature, 471, 212–217.

Christiansen, E. H. (2005) Contrasting processes in silicic magma chambers: evidence from very large volume ignimbrites. Geological Magazine, 42, 669–681.

Claiborne, L.L., Miller, C.F., Walker, B.A., Wooden, J.L., Mazdab, F.K., and Bea, F., 2006, Tracking magmatic processes through Zr/Hf ratios in rocks and Hf and Ti zoning in zircons: An example from the Spirit Mountain batholith, Nevada. Mineralogical Magazine, 70, 517–543.

Claiborne, L. L., Miller, C.F., and Wooden, J.L. (2010) Trace element composition of igneous zircon: a thermal and compositional record of the accumulation and evolution of a large silicic batholith, Spirit Mountain, Nevada. Contributions to Mineralogy and Petrology, 160, 511–531.

Coint, N. Barnes, C.G., Yoshinobu, A.S, Chamberlain, K.R. and Barnes, M.A. (2013a) Batch-wise assembly and zoning of a tilted calc-alkaline batholith: Field relations, timing, and compositional variation. Geosphere, 9, 1729–1746.

Coint, N., Barnes, C.G., Yoshinobu, A.S., Barnes, M.A. and Buck, S. (2013b) Use of trace element abundances in augite and hornblende to determine the size of the connectivity, timing, and evolution of magma batches in a tilted batholith. Geosphere, 9, 1747–1765.

Coleman, D. S., and Glazner, A. F. (1997) The Sierra Crest magmatic event: rapid formation of juvenile crust during the Late Cretaceous in California. International Geology Review, 39, 768–787.

Coleman, D.S., Gray, W., and Glazner, A.F. (2004) Rethinking the emplacement and evolution of zoned plutons: Geochronologic evidence for incremental assembly of the Tuolumne Intrusive Suite, California. Geology, 32, 433–436.

Coleman, D.S., Bartley, J.M., Glazner, A.F., and Pardue, M.J. (2012) Is chemical zonation in plutonic rocks driven by changes in source magma composition or shallow-crustal differentiation? Geosphere, 8, 1568–1587.

Colombini, L.L., Miller, C.F., Gualda, G.A.R., Wooden, J.L., and Miller, J.S. (2011) Sphene and zircon in the Highland Range volcanic sequence (Miocene, southern Nevada, USA): elemental partitioning, phase relations, and influence on evolution of silicic magma. Mineralogy and Petrology, 102, 29–50.

Ducea, M., (2001) The California arc: thick granitic batholiths, eclogitic residues, lithospheric-scale thrusting, and magmatic flare-ups. GSA Today, 11, 4–10

Economos, R.C., Memeti, V., Paterson, S.R., Miller, J.S., Erdmann, S., and Žák, J. (2010) Causes of compositional diversity in a lobe of the Half Dome granodiorite, Tuolumne

Batholith, central Sierra Nevada, California. Earth and Environmental Science Transactions of the Royal Society of Edinburgh, 100, 173–183.

Esawi, E.K. (2004) AMPH-CLASS: An Excel spreadsheet for the classification and nomenclature of amphiboles based on the 1997 recommendations of the International Mineralogical Association. Computers & Geosciences, 30, 753–760.

Gelman, S.E., Gutiérrez, F.J., and Bachmann, O. (2013) On the longevity of large upper crustal silicic magma reservoirs. Geology, 41, 759–762.

Gelman, S.E., Deering, C.D., Bachmann, O., Huber, C., and Gutiérrez, F. (2014) Identifying the crystal graveyards remaining after large silicic eruptions. Earth and Planetary Science Letters, 403, 299–306.

Graeter, K.A., Beane, R.J., Deering, C.D., Gravley, D.M., and Bachmann, O. (2015) Formation of rhyolite at the Okataina Volcanic Complex, New Zealand: New insights from analysis of quartz clusters in plutonic lithics. American Mineralogist, 100, 1778–1789.

Glazner, A.F., and Bartley, J.M. (2006) Is stoping a volumetrically significant pluton emplacement process? Geological Society of America Bulletin, 118, 1185–1195.

Glazner, A.F., Bartley, J.M., Coleman, D.S., Gray, W., and Taylor, G.K. (2004) Are plutons assembled over millions of years by amalgamation from small magma chambers? GSA Today, 14, 4–11.

Gray, W., Glazner, A.F., Coleman, D.S., and Bartley, J.M. (2008) Long-term geochemical variability of the Late Cretaceous Tuolumne Intruisve Suite, central Sierra Nevada, California. Geological Society, London, Special Publication, 304, 183–201.

Greenland, L.P. (1970) An equation for trace element distribution during magmatic crystallization. American Mineralogist 55, 455–465.

Huber, N.K., Bateman, P.C., and Wahrhaftig, C. (1989) Geologic map of Yosemite National Park and vicinity, California. Miscellaneous Investigations Series I-1874, U.S. Geological Survey, 1:125,000.

Johnson, M.C., and Rutherford, M.J. (1989) Experimental calibration of the aluminum-in-hornblende geobarometer with application to Long Valley caldera (California) volcanic rocks. Geology, 17, 837-841.

Kistler, R. W., and Fleck, R. J. (1994) Field guide for a transect of the central Sierra Nevada, California: geochronology and isotope geology. US Geological Survey Open-File Report, 94-0267.

Kistler, R.W., Chappell, B.W., Peck, D.L., and Bateman, P.C. (1986) Isotopic variation in the Tuolumne Intrusive Suite, central Sierra Nevada, California. Contributions to Mineralogy and Petrology, 94, 205–220.

Klein, M., Stosch, H.G., and Seck, H.A. (1997) Partitioning of high field strenght elements between amphibole and quartz-dioritic to tonalitic melts: an experimental study. Chemical Geology, 138, 257–271.

Leake, B.E., Woolley, A.R., Arps, C.E.S., Birch, W.D., Gilbert, M.C., Grice, J.D., Hawthorne, F.C., Kato, A., Kisch, H.J., Krivovichev, V.G., Linthout, K., Laird, J., Mandarino, J.A., Maresch, W.V., Nickel, E.H., Rock, N.M.S., Schumacher, J.C., Smith, D.C., Stephenson, N.C.N., Ungaretti, L., Whittaker, E.J.W., and Youzhi, G. (1997) Nomenclature of amphiboles: report of the subcommittee on amphiboles of the International Mineralogical Association Commission on new minerals and mineral names. Canadian Mineralogist, 35, 219–246.

This is a preprint, the final version is subject to change, of the American Mineralogist (MSA)
Cite as Authors (Year) Title. American Mineralogist, in press.
(DOI will not work until issue is live.) DOI: http://dx.doi.org/10.2138/am-2016-5383 10/7

Lipman, P.W., and Bachmann, O. (2015) Ignimbrites to batholiths: Integrating perspectives from geological, geophysical, and geochronological data. Geosphere, 11, 705–743.

Mattinson, J.M. (2005) Zircon U–Pb chemical abrasion ("CA-TIMS") method: Combined annealing and multi-step partial dissolution analysis for improved precision and accuracy of zircon ages. Chemical Geology, 220, 47–66.

Matzel, J.E.P., Bowring, S.A., and Miller, R.B. (2006) Time scale of pluton construction at differing crustal levels: examples from the Mount Stuart and Tenpeak intrusions, North Cascades, Washington. Geological Society of America Bulletin, 118, 1412–1430.

Memeti, V., Krause, J., Anderson, J.L., Paterson, S.R. (2009) Interpreting Al-in Hornblende and Hbl-Plag thermobarometry results from the Tuolumne batholith and magmatic lobes in conjunction with single mineral element distribution electron microprobe maps. Eos Transactions of the American Geophysical Uunion, 90(52), Fall Meet. Suppl., # V42A-06.

Memeti, V., Paterson, S., Matzel, J., Mundil, R., and Okaya, D. (2010) Magmatic lobes as “snapshots” of magma chamber growth and evolution in large, composite batholiths: An example from the Tuolumne intrusion, Sierra Nevada, California. Geological Society of America Bulletin, 122, 1912–1931.

Memeti, V., Paterson, S., and Mundil, R. (2014) Day 4: Magmatic evolution of the Tuolumne Intrusive Complex, *in* Memeti, V., Paterson, S.R., and Putirka, K.D., eds., Formation of the Sierra Nevada Batholith: Magmatic and tectonic processes and their tempos. Geological Society of America Field Guide, 34, 43–74, doi:10.1130/2014.0034(04).

Michel, J., Baumgartner, L., Putlitz, B., Schaltegger, U., and Ovtcharova, M. (2008) Incremental growth of the Patagonian Torres del Paine laccolith over 90 k.y. Geology, 36, 459–462.

Miller, J.S., Matzel, J.E.P., Miller, C.F., Burgess, S.D., and Miller, R.B. (2007) Zircon growth and recycling during the assembly of large composite arc plutons. Journal of Volcanology and Geothermal Research, 167, 282–299.

Naney, M.T. (1983) Phase equilibria of rock-forming ferromagnesian silicates in granitic systems. American Journal of Science, 283, 993–1033.

Paterson, S.R., Fowler, K.T., Schmidt, K.L., Yoshinobu, A.S., and Miller, R.B. (1998) Interpreting magmatic fabric patterns in plutons. Lithos, 44, 53–82.

Paterson, S.R., Okaya, D., Memeti, V., Economos, R., and Miller, R.B. (2011) Magma addition and flux calculations of incrementally constructed magma chambers in continental margin arcs: Combined field, geochronologic, and thermal modeling studies. Geosphere, 7, 1439–1468.

Putirka, K. (in review), Amphibole thermometers and barometers for igneous systems, and some implications for eruption mechanisms of felsic magmas at arc volcanoes. American Mineralogist.

Piwinskii, A.J., 1973a, Experimental studies of granitoids from the central and southern Coast Ranges, California: Tschermaks. Min. Petr. Mitt., v. 20, p. 107-130.

Piwinskii, A.J., 1973b, Experimental studies of igneous rock series, central Sierra Nevada batholith, California: Part II: N. Jb. Miner. Mh., v. 5, p. 193-215.

Schaltegger, U., Brack, P., Ovtcharova, M., Peytcheva, I., Schoene, B., Stracke, A., Marocchi, M., and Bargossi, G.M. (2009) Zircon and titanite recording 1.5 million years of magma accretion, crystallization and initial cooling in a composite pluton (southern Adamello batholith, northern Italy). Earth and Planetary Science Letters. 286, 208–218.

Schmidt, M.W. (1992) Amphibole composition in tonalite as a function of pressure: an experimental calibration of the Al-in-hornblende barometer. Contributions to Mineralogy and Petrology, 110, 304–310.

Schoene, B., Guex, J., Barolini, A., Schaltegger, U., and Blackburn, T.J. (2010) Correlating the end-Triassic mass extinction and flood basalt volcanism at the 100 ka level. Geology, 38, 387–390.

Schoene, B., Schaltegger, U., Brack, P., Latkoczy, C., Stracke, A., and Günther, D. (2012) Rates of magma differentiation and emplacement in a ballooning pluton recorded by U–Pb TIMS-TEA, Adamello batholith, Italy. Earth and Planetary Science Letters, 355–356, 162–173.

Sisson, T.W. (1994) Hornblende-melt trace-element partitioning measured by ion microprobe. Chemical Geology, 117, 331–344.

Stepanov, A.S., and Hermann, J., (2013) Fractionation of Nb and Ta by biotite and phengite: Implications for the “missing Nb paradox”. Geology, 41, 303–306.

Sun, S.-S., and McDonough, W.F. (1989) Chemical and isotopic systematics of oceanic basalts: implications for mantle composition and processes, *in* Saunders, A.D., and Norry, M.J., eds., Magmatism in the ocean basins. Geological Society Special Publication, 42, 313-345.

Tappa, M.J., Coleman, D.S., Mills, R.D., and Samperton, K.M. (2011) The plutonic record of a silicic ignimbrite from the Latir volcanic field, New Mexico. Geochemistry Geophysics Geosystems, 12.

Tiepolo, M., and Vannucci, R. (2014) The contribution of amphibole from deep arc crust to the silicate Earth’s Nb budget. Lithos, 208–209, 16–20.

Tiepolo, M. Oberti, R., Zanetti, A., Vannucci, R., and Foley, S.F. (2007) Trace-element partitioning between amphibole and silicate melt, *in* Hawthorne, F.C., Oberti, R., Ventura, G.D., and Mottana, A. eds., Amphiboles: Crystal Chemistry, Occurrence, and Health Issues, Reviews in Mineralogy and Geochemistry, 67, 417–452.

Ward, K.M., Zandt, G., Beck, S.L., Christensen, D.H., and McFarlin, H. (2014) Seismic imaging of the magmatic underpinnings beneath the Altiplano-Puna volcanic complex from the joint inversion of surface wave dispersion and receiver functions. Earth and Planetary Science

Yuan, X., Sobolev, S.V., Kind, R., Oncken, O., Bock, G., G. Asch, Schurr, B., Graeber, F., Rudloff, A., Hanka, W., Wylegalla, K., Tibi, R., Haberland, C., Rietbrock, A., Giese, P., Wigger, P., RoÈwer, P., Zandt, G., Beck, S., Wallace, T., Pardo, M., and Comte, D. (2000) Subduction and collision processes in the Central Andes constrained by converted seismic phases. Nature, 408, 958–961.

Žák, J., and Paterson, S.R. (2005) Characteristics of internal contacts in the Tuolumne Batholith, central Sierra Nevada, California (USA): Implications for episodic emplacement and physical processes in a continental arc magma chamber. Geological Society of America Bulletin, 117, 1242–1255, doi: 10.1130/B25558.1.

Žák, J., Paterson, S. R., and Memeti, V. (2007) Four magmatic fabrics in the Tuolumne batholith, central Sierra Nevada, California (USA): Implications for interpreting fabric patterns in plutons and evolution of magma chambers in the upper crust. Geological Society of America Bulletin, 119, 184–201, doi:10.1130/B25773.

Figure captions

Figure 1 Simplified geologic map of the Tuolumne Intrusive Complex modified after Huber et al. (1989) and Memeti et al. (2014). Inset box shows the location of the Kuna Crest lobe (Fig. 2).

Figure 2. Geologic map of the Kuna Crest lobe with locations of samples used in this study.

Figure 3.Simplified geologic map of the Wooley Creek batholith with locations of samples used in this study (after Coint et al., 2013a).

Figure 4. Photomicrographs. Horizontal field of view is 2 mm in all images. A. Hornblende enclosing relict augite and Fe-Ti oxides. Round spots in the hornblende are 40μ-diameter laser ablation pits. B. The range of hornblende habits in the KCL is illustrated by prismatic, intergranular, and subpoikilitic hornblende in this sample. C. A cluster of prismatic hornblende and titanite. Note inclusions of Fe-Ti oxides and apatite in the hornblende. D. Large hornblende grains are Cr-poor 'phenocrysts' in mafic enclave KCL-16B; the small hornblende grains are Cr-rich groundmass crystals. E. Poikilitic amphibole in central hybrid sample KCL-536. Note the partial replacement of olive hornblende by paler, blue-green actinolitic amphibole. F. A cluster of prismatic hornblende, magnetite, biotite, and titanite in central hybrid sample KCL-536.

Figure 5. Variation of CaO versus Sr in bulk-rock samples for the Tuolumne Intrusive Complex and upper zone of the Wooley Creek batholith. The symbols represent published data for the Tuolumne Intrusive complex (Bateman and Chappell, 1979; Burgess and Miller, 2008; Gray et

al., 2008; Economos et al., 2008; Coleman et al., 2012; and Memeti et al., this volume). Numbers associated with Kuna Crest data points indicate samples analyzed in this study. Data for the upper zone and dacitic roof dikes of the Wooley Creek batholith are from Coint et al. (2013a).

Figure 6. Compositional ranges of hornblende from the Kuna Crest lobe, one sample from the equigranular Half Dome Granodiorite, the upper Wooley Creek batholith (WCB), and the Fish Canyon Tuff (Bachmann and Dungan, 2002). Data plotted in cations per formula unit. Data for WCB hornblende are from Barnes (1987) and Coint et al. (2013b). Data for the Tuolumne Intrusive Complex are from Gray et al. (2008) and this paper. The vertically-lined field in (A) represents hornblende from the tonalitic host to an enclave swarm in the upper WCB.

Figure 7. Trace element variation in hornblende. Symbols represent spot analyses. The pale gray field encloses hornblende compositions from the upper zone of the Wooley Creek batholith and dacitic roof-zone dikes (Coint et al., 2013b); the dark gray field represents analyses from a single upper-zone sample (MMB-317; Coint et al., 2013b). Gray arrows indicate compositional trends from crystal interiors to rims. Gray inverted triangles indicate data for phenocrysts in the mafic enclave, all of which have < 40 ppm Cr. Black triangles represent groundmass grains which have Cr contents from 63–350 ppm. The field labeled ‘actinolitic’ represents pale green to blue-green actinolitic decorations and replacement zones in hornblende. A. Sr versus Ti. B. Nb versus Ti. Note the increase in Nb from crystal interiors to rims in sample VLM-2 from the KCL tip at Waugh Lake. C. Zr versus Hf. The reference line at Zr:Hf = 20:1 is the Zr/Hf ratio expected in hornblende crystallized from melt with chondritic Zr/Hf ratio. D. Ta versus Nb. E. Ce versus Hf. F. Ba versus Ti. In panels C, D, and E, the dashed lines are fractional crystallization trends, with

numbers adjacent to the small gray and black squares indicating the values of F, fraction of melt remaining assuming constant bulk distribution coefficients.

Figure 8. Representative chondrite-normalized (Sun and McDonough, 1989) rare earth element diagrams for hornblende from the Tuolumne Intrusive Complex. Data for the upper Wooley Creek batholith plotted in panel A are from Coint et al. (2013b).

Table 1. Representative bulk-rock compositions

sample	VLM-2	KCL-390	KCL-434-2	KCL-536	KCL-214
major oxides in weight %					
SiO2	59.46	59.92	62.33	63.43	65.48
TiO2	0.81	0.86	0.76	0.70	0.52
Al2O3	17.53	16.94	17.69	16.15	15.52
FeO total	6.48	6.51	4.32	4.90	3.71
MnO	0.13	0.11	0.08	0.08	0.08
MgO	2.68	3.09	1.80	2.18	1.60
CaO	6.12	6.02	4.96	4.52	3.79
Na2O	3.76	3.56	3.80	3.36	3.48
K2O	2.18	2.27	3.57	3.50	3.52
P2O5	0.26	0.22	0.21	0.20	0.16
SUM	99.40	99.50	99.52	99.02	97.85
Mg/(Mg+Fet)**	0.42	0.46	0.43	0.44	0.43
trace elements in parts per million					
Ni	13.4	19.7	13.9	13.8	1.0
Cr	4.4	20.7	13.6	11.4	4.8
Sc	12.13	16.65	10.94	8.79	6.11
V	139.2	161.3	96.4	110.1	77.9
Ba	914	546	1143	953	864
Rb	62.6	104.0	91.4	137.16	125.46
Sr	628.4	531.1	526.1	546.95	489.32
Zr	132.4	154.7	229.0	143.09	110.73
Y	22.89	18.44	17.06	14.98	13.17
Nb	8.47	7.92	9.75	6.95	8.40
Ga	19.1	20.3	19.7	17.9	18.2
Cu	13.1	35.1	22.2	11.2	7.0
Zn	86.6	83.8	66.6	75.2	61.5
La	21.8	23.8	23.3	24.1	26.0

Ce	43.1	44.4	43.2	44.7	50.8
Pr	5.3	5.0	5.0	5.0	5.9
Nd	23.0	20.0	20.3	19.1	21.6
Sm	5.4	4.5	4.5	4.1	4.2
Eu	1.30	1.16	1.35	1.05	1.01
Gd	4.67	4.00	3.91	3.40	3.27
Tb	0.74	0.61	0.57	0.51	0.47
Dy	4.26	3.47	3.23	2.82	2.64
Ho	0.83	0.67	0.61	0.53	0.49
Er	2.19	1.79	1.61	1.42	1.29
Tm	0.31	0.25	0.22	0.20	0.19
Yb	1.93	1.60	1.37	1.27	1.20
Lu	0.30	0.26	0.23	0.20	0.20
Pb	9.68	12.25	17.41	14.59	17.74
Cs	2.18	8.19	3.18	7.36	6.30
U	0.97	4.64	2.05	5.27	7.52
Th	4.77	13.42	6.36	17.97	33.56
Hf	3.64	4.47	5.91	4.30	3.56
Ta	0.54	0.80	0.67	0.70	0.99

VLM-2	granodiorite from the Waugh Lake pluton, southern KCL tip
KCL-390	granodiorite from KCL unit III
KCL-434-2	tonalite from KCL unit I
KCL-536A	granodiorite from the hybrid zone between KCL and eHD
KCL-214	granodiorite of the eHD

Table 2. Representative hornblende compositions.

sample #	KCL434-2---lobe unit I				KCL390B--lobe unit III				KCL536-- I
rock type	tonalite				granodiorite				
grain #	C3-3-1-1	C3-3-4-1	C2-2-3-1	C2-2-4-1	4-2-1	4-3-1	6-2-1	6-5-1	16b-c1
notes	rim	poik hb	prism rim	prism rim	core	rim	core	rim	inner rim
major oxides in weight %									
SiO2	48.21	46.84	47.88	47.56	46.06	46.23	46.05	46.53	46.98
TiO2	1.18	1.33	1.07	1.10	1.31	1.30	1.23	1.31	1.21
Al2O3	6.06	6.25	6.16	6.30	7.70	7.54	7.28	7.67	7.24
FeO	14.92	15.35	15.58	15.48	16.87	16.93	16.40	16.77	15.73
MnO	0.50	0.55	0.51	0.48	0.49	0.46	0.46	0.43	0.46
MgO	13.56	13.09	12.90	13.08	11.86	12.02	12.14	11.96	12.63
CaO	11.57	11.44	11.77	11.76	11.65	11.66	11.62	11.64	11.63
Na2O	0.89	1.11	0.94	0.90	1.00	1.02	0.93	1.01	1.15
K2O	0.59	0.67	0.63	0.66	0.85	0.86	0.76	0.82	0.81
Cl	0.07	0.11	0.09	0.10	0.13	0.13	0.10	0.13	0.13
F	0.26	0.00	0.21	0.10	0.13	0.04	0.03	0.07	0.17
Sum	97.71	96.78	97.67	97.49	98.01	98.19	97.02	98.34	98.10
trace elements in ppm									
P	20.4	22.0	34.6	39.1	57.9	58.5	32.2	33.8	43.4
Sc	146.5	126.3	183.2	198.4	118.8	112.5	120.4	100.5	77.3
Ti	8680	9704	8755	8645	9390	9345	8864	9313	8861
V	253.9	276.2	224.0	216.1	340.6	335.6	325.9	328.3	259.4
Cr	bdl	11.9	6.9	9.5	33.7	48.5	30.8	31.4	18.7
Mn	4177	4498	3646	3782	3649	3602	3456	3549	3568
Sr	22.67	24.79	20.44	22.59	43.01	42.49	38.43	41.04	29.94
Y	215.46	219.61	177.80	183.34	110.36	105.44	113.87	95.39	24.36
Zr	25.53	26.70	25.61	26.47	33.55	32.99	33.19	32.28	27.22
Nb	28.78	29.34	26.61	26.98	26.74	26.38	25.24	25.81	11.74
Ba	11.83	12.47	10.88	11.94	31.32	32.33	28.29	28.88	11.01
La	35.05	38.12	34.97	36.28	50.61	49.66	45.81	47.21	20.84
Ce	167.11	180.58	147.77	152.28	200.03	194.64	175.72	175.09	54.93
Pr	30.96	33.04	27.46	28.26	30.75	29.15	28.24	26.67	7.40

Nd	154.95	160.53	135.28	138.49		131.02	124.07	123.06	112.56		29.28
Sm	47.36	49.20	39.12	40.37		30.60	28.93	28.69	24.05		5.64
Eu	3.53	3.89	3.74	3.75		3.81	3.77	3.47	3.62		0.83
Gd	46.08	46.49	38.64	38.15		25.35	24.42	25.10	21.29		5.56
Tb	6.95	7.21	5.82	5.84		3.60	3.51	3.65	3.12		0.67
Dy	43.15	43.35	35.70	36.89		21.71	21.13	22.59	18.35		4.37
Ho	8.30	8.55	6.76	7.03		4.14	3.91	4.25	3.45		0.89
Er	23.53	23.72	19.41	19.89		11.55	10.98	12.67	10.17		2.35
Tm	3.01	3.19	2.56	2.71		1.73	1.68	1.69	1.43		0.35
Yb	19.75	20.43	16.66	17.05		12.17	11.81	11.98	9.53		2.81
Lu	2.45	2.77	2.17	2.36		1.70	1.64	1.70	1.32		0.51
Hf	2.13	1.97	2.00	1.80		3.03	2.60	2.83	2.60		2.35
Ta	1.49	1.51	1.48	1.45		2.27	2.23	2.14	2.16		0.24
Pb	1.63	1.94	1.44	1.55		2.69	2.60	2.10	2.67		1.62
Th	0.13	0.27	0.25	0.25		0.38	0.40	0.38	0.45		0.21
U	bdl	0.23	0.06	0.14		0.39	0.42	0.26	0.39		0.13

Kuna Crest-eHD hybrid granodiorite		VLM-2---Waugh Lake pluton granodiorite			KCL16B---mafic magmatic enclave			
16-d1	16-b1	4h	4h	4h	20-e1	20-c1	26-d1	26-x1-1
mantle	inner rim	rim	core	poikilitic	term	core		gm xtal
46.25	46.33	44.99	46.23	46.60	45.39	46.03	45.83	47.28
1.34	1.26	2.00	1.63	1.46	1.51	1.47	1.37	1.28
7.43	7.43	8.47	7.54	7.22	8.47	8.33	8.14	7.03
15.95	15.80	16.63	15.68	15.87	15.07	13.77	15.12	14.81
0.47	0.47	0.56	0.62	0.57	0.35	0.35	0.28	0.32
12.19	12.39	12.02	12.65	12.90	12.61	13.67	12.34	13.14
11.55	11.66	11.79	11.58	11.71	11.59	11.49	11.87	11.81
0.98	1.08	1.21	1.20	0.96	1.28	1.35	0.99	0.96
0.84	0.86	0.90	0.79	0.75	0.86	0.65	0.83	0.68
0.11	0.13	0.07	0.05	0.05	0.12	0.10	0.10	0.09
0.17	0.30	-	-	-	0.28	0.18	0.10	0.22
97.23	97.61	98.62	97.96	98.09	97.44	97.35	96.95	97.55
44.2	39.6	38.6	46.6	44.9	84.6	50.9		72.6
125.7	104.6	66.4	140.9	173.4	74.0	99.1		74.6
9478	9440	10354	13111	13669	10185	11784		12347
250.2	244.6	235.5	256.3	268.9	345.6	360.5		419.5
3.8	5.7	2.8	bdl	bdl	33.1	37.4		208.4
3544	3461	4445	3813	3568	2344	2984		2358
34.95	34.30	53.79	69.55	76.17	69.78	73.08		130.94
74.73	60.54	107.45	191.39	235.42	96.07	120.48		42.90
27.51	26.85	46.35	55.83	58.72	39.33	46.10		47.28
19.61	17.75	31.37	23.37	22.84	21.36	24.66		7.46
15.43	13.01	67.00	160.26	176.76	54.92	60.54		171.50
23.52	21.72	38.18	35.70	36.17	26.77	25.14		28.83
88.35	79.01	136.33	144.02	156.96	104.56	104.78		95.00
14.87	12.70	23.03	28.14	31.77	17.85	19.16		12.65

66.12	55.20	104.36	146.59	174.60	82.24	92.96	50.72
16.23	13.06	23.37	42.22	54.23	23.16	28.00	10.80
1.95	1.56	3.05	4.49	4.99	2.97	3.69	2.99
14.98	11.56	19.77	43.17	54.94	20.97	25.75	8.98
2.08	1.72	2.98	6.21	8.33	3.22	4.02	1.35
12.58	10.20	19.28	40.09	52.60	19.71	24.79	8.61
2.61	2.03	3.79	7.54	9.50	3.67	4.76	1.50
7.97	6.24	12.11	21.11	25.44	10.19	13.23	4.64
1.20	0.96	1.90	2.89	3.21	1.41	1.78	0.70
8.23	7.24	12.98	17.81	18.67	9.00	11.54	4.98
1.30	1.15	1.73	2.27	2.36	1.18	1.44	0.77
2.62	2.43	2.98	3.05	3.30	2.57	3.03	2.18
0.69	0.56	1.19	0.87	0.82	1.35	1.36	0.28
2.05	1.66	1.42	1.44	1.45	2.10	2.59	2.83
0.33	0.54	0.33	0.24	0.29	0.56	0.45	0.59
0.12	0.32	0.06	0.08	0.10	0.34	0.17	0.39

Table 3. Examples of fractional crystallization models.

	Ba	Sr	Zr	Hf	Nb	Ta	Ce
Kuna Crest lobe zone III							
d	0.16	0.3	0.5	1	2–3	1.5	3.2–4.2
D	2.5	2.0	2.5	2.5	2.0	2.0	2.5
c(melt)	220	150	80	3.6	9.7–14	1.6	52.4–68.8
c(rock)	546	531	155	4.47	7.9	0.8	44.4
reference	1	1	3	1	3	---	1, 2
	cumulate biotite?	cumulate plag	cumulate zircon	cumulate zircon	dilution	dilution	dilution
upper Wooley Creek batholith (sample MMB-317)							
d	0.16	0.3	0.6	1	1	0.5	2
D	2.5	2.2	2.0	1.8	2.0	2.0	1.5
c(melt)	1250	65	142	4.2	17	1.2	37.5
c(rock)	729	438	128	2.89	6	1	24
reference	1	1	2	1	1, 3	3	2
	dilution	cumulate plag	dilution	dilution	dilution	dilution	dilution

d, hornblende/melt partition coefficient; D, bulk partition coefficient
c(melt), calculated concentration in melt at beginning of hornblende crystallization (ppm)
c(rock), bulk-rock concentration (ppm)

References:

1. Klein et al. (1997)
2. Sisson (1994)
3. Bachmann et al. (2005)

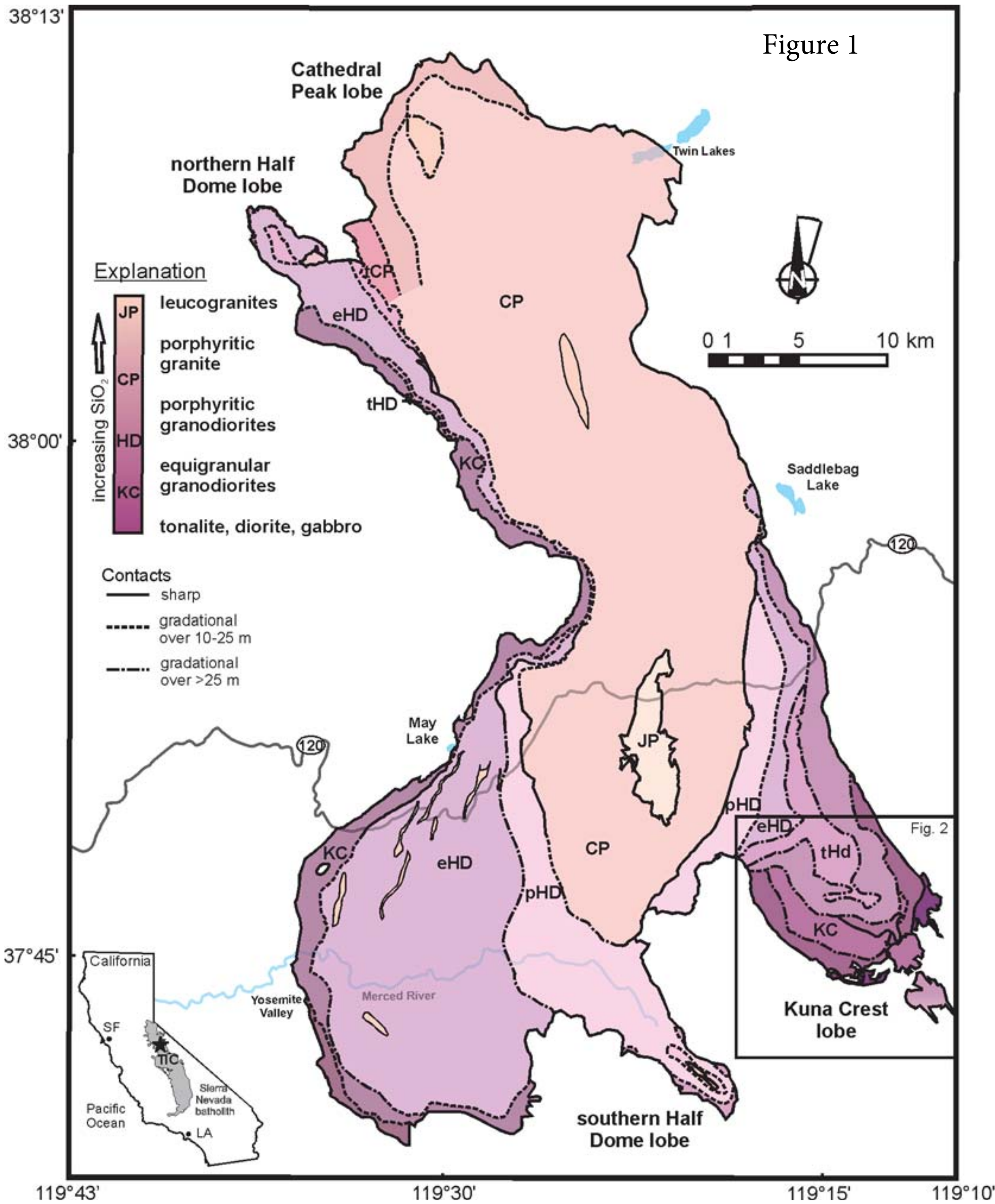
Figure 1
Cathedral Peak lobe
northern Half Dome lobe
Twin Lakes
Explanation
JP
CP
HD
KC
increasing SiO2
leucogranites
porphyritic granite
porphyritic granodiorites
equigranular granodiorites
tonalite, diorite, gabbro
Contacts
sharp
gradational over 10-25 m
gradational over >25 m
tCP
eHD
tHD
KC
CP
0 1 5 10 km
Saddlebag Lake
120
May Lake
JP
pHD
eHD
tHd
Fig. 2
KC
Kuna Crest lobe
Merced River
Yosemite Valley
southern Half Dome lobe
California
SF
TIC
Sierra Nevada batholith
Pacific Ocean
LA
38°13'
38°00'
37°45'
119°43'
119°30'
119°15'
119°10'

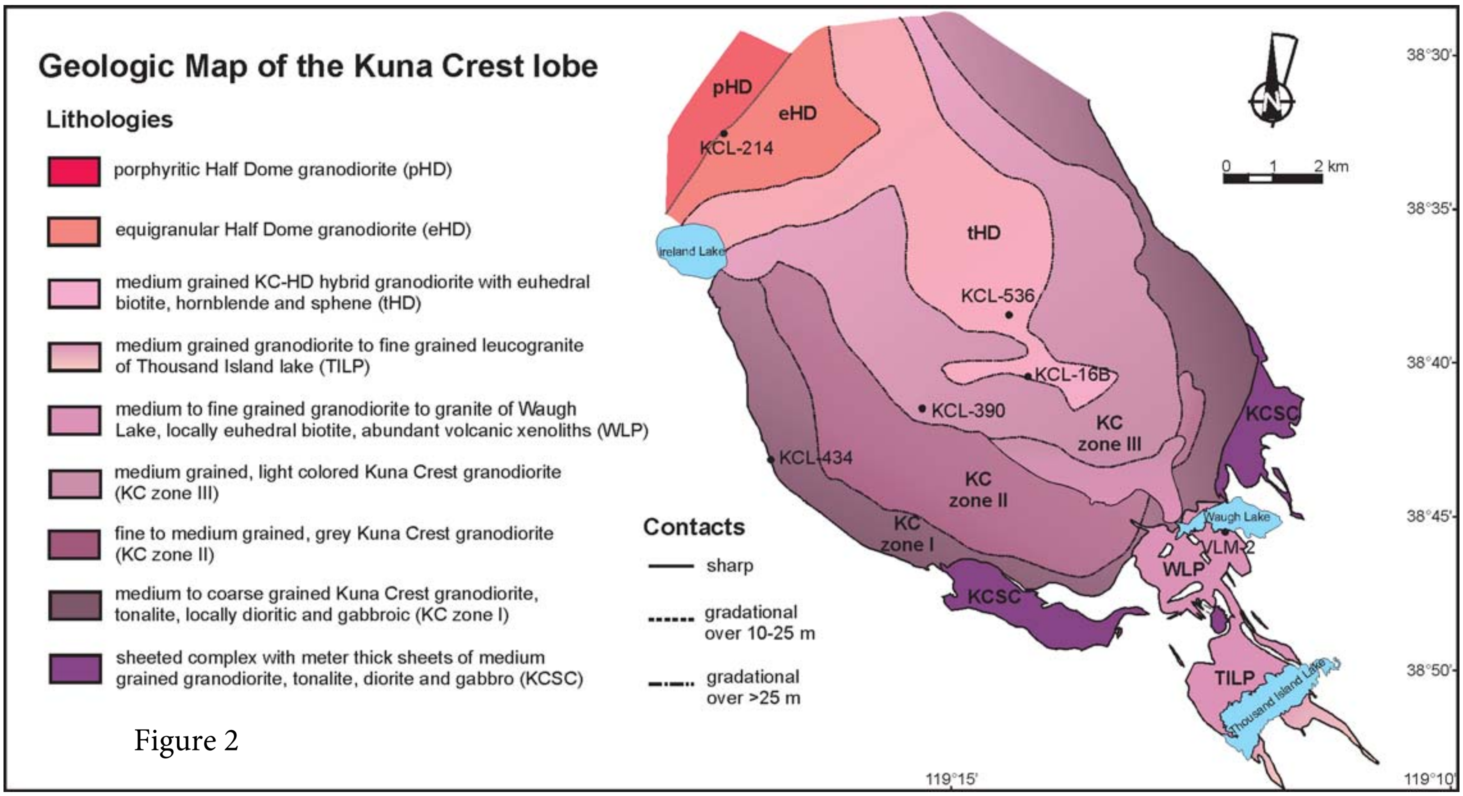
Geologic Map of the Kuna Crest lobe
Lithologies
porphyritic Half Dome granodiorite (pHD)
equigranular Half Dome granodiorite (eHD)
medium grained KC-HD hybrid granodiorite with euhedral biotite, hornblende and sphene (tHD)
medium grained granodiorite to fine grained leucogranite of Thousand Island lake (TILP)
medium to fine grained granodiorite to granite of Waugh Lake, locally euhedral biotite, abundant volcanic xenoliths (WLP)
medium grained, light colored Kuna Crest granodiorite (KC zone III)
fine to medium grained, grey Kuna Crest granodiorite (KC zone II)
medium to coarse grained Kuna Crest granodiorite, tonalite, locally dioritic and gabbroic (KC zone I)
sheeted complex with meter thick sheets of medium grained granodiorite, tonalite, diorite and gabbro (KCSC)
Contacts
sharp
gradational over 10-25 m
gradational over >25 m
pHD
eHD
KCL-214
Ireland Lake
tHD
KCL-536
KCL-16B
KCL-390
KCL-434
KC zone III
KC zone II
KC zone I
KCSC
Waugh Lake
VLM-2
WLP
TILP
Thousand Island Lake
0 1 2 km
38°30'
38°35'
38°40'
38°45'
38°50'
119°15'
119°10'
Figure 2

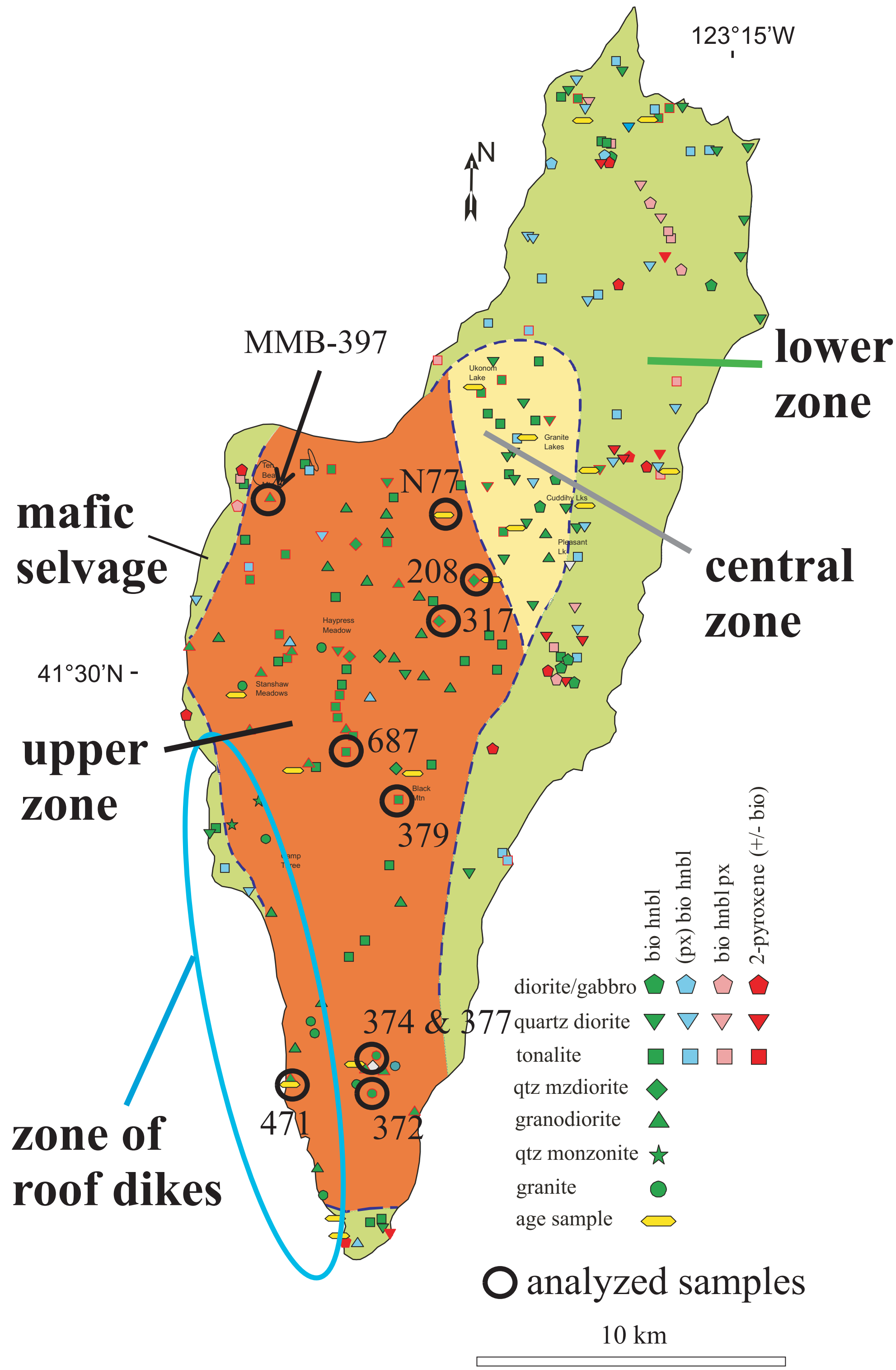
123°15'W
N
lower zone
MMB-397
N77
mafic selvage
208
317
central zone
41°30'N
upper zone
687
379
zone of roof dikes
374 & 377
471
372
bio hnbl
(px) bio hnbl
bio hnbl px
2-pyroxene (+/- bio)
diorite/gabbro
quartz diorite
tonalite
qtz mzdiorite
granodiorite
qtz monzonite
granite
age sample
analyzed samples
10 km

Figure 3

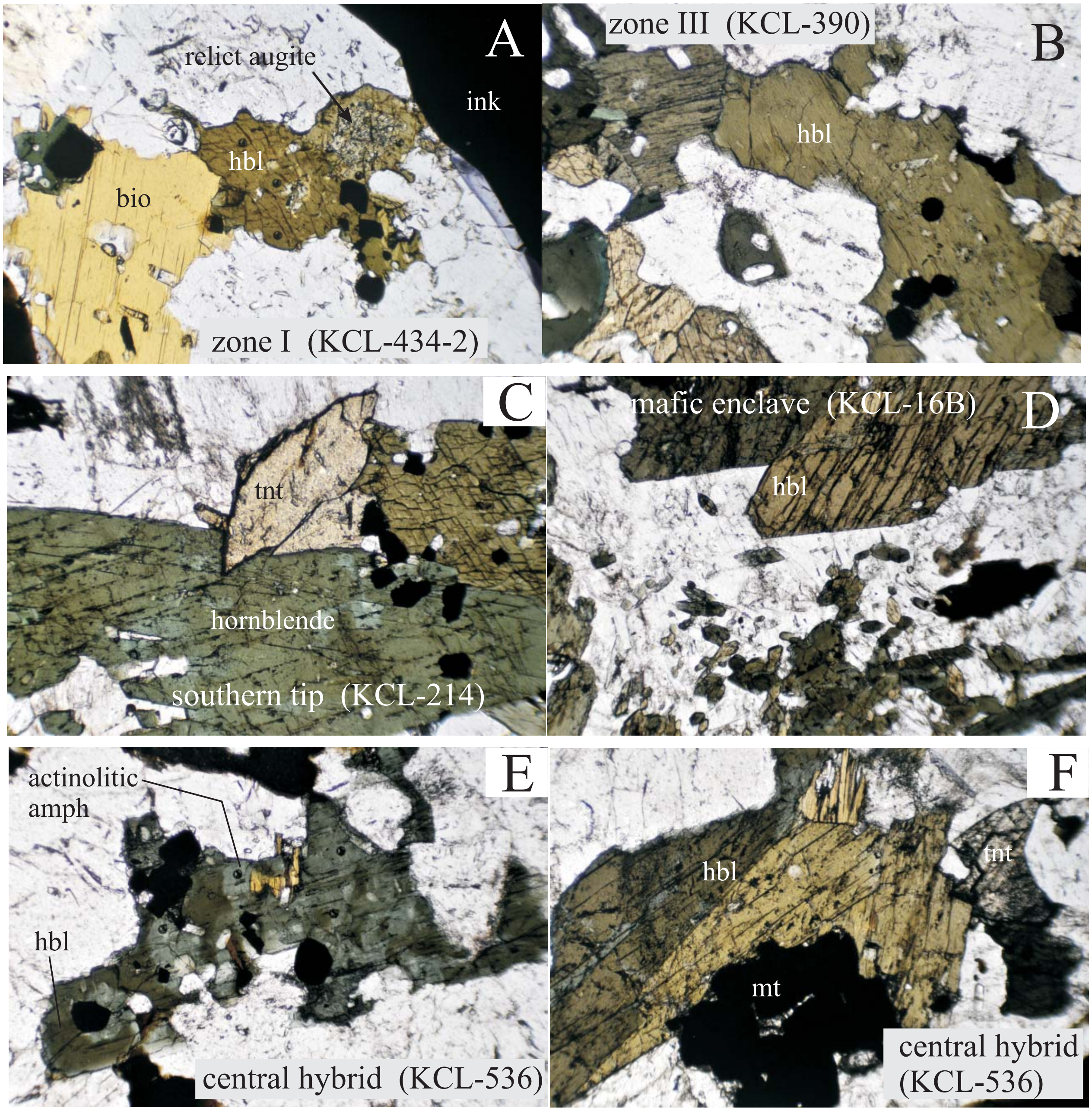
A
relict augite
ink
hbl
bio
zone I (KCL-434-2)
zone III (KCL-390)
B
hbl
C
tnt
hornblende
southern tip (KCL-214)
mafic enclave (KCL-16B)
D
hbl
E
actinolitic
amph
hbl
central hybrid (KCL-536)
F
hbl
tnt
mt
central hybrid
(KCL-536)

Figure 4.

This is a preprint, the final version is subject to change, of the American Mineralogist (MSA)
Cite as Authors (Year) Title. American Mineralogist, in press.
(DOI will not work until issue is live.) DOI: http://dx.doi.org/10.2138/am-2016-5383

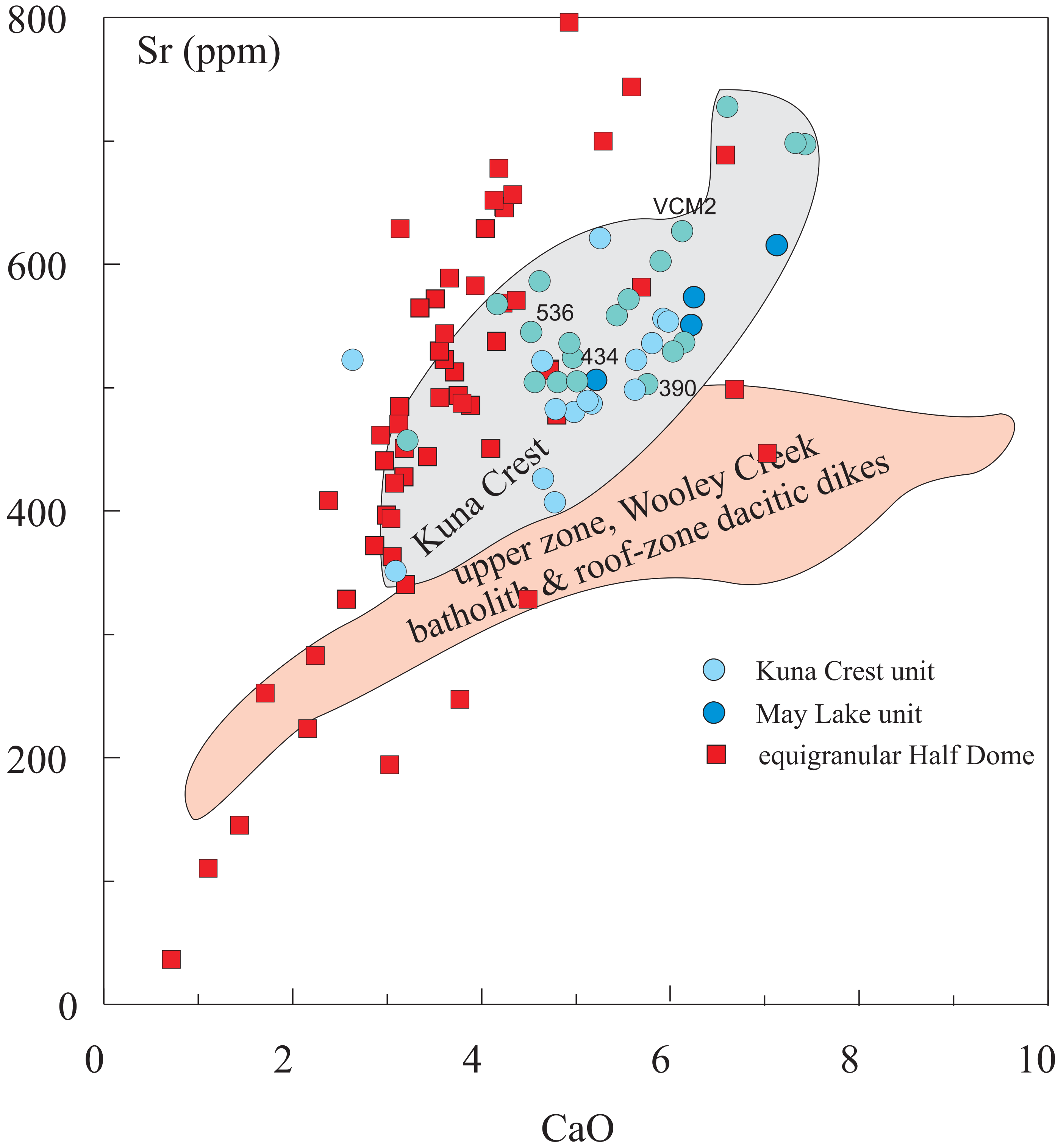

Figure 5.

This is a preprint, the final version is subject to change, of the American Mineralogist (MSA)
Cite as Authors (Year) Title. American Mineralogist, in press.
(DOI will not work until issue is live.) DOI: http://dx.doi.org/10.2138/am-2016-5383

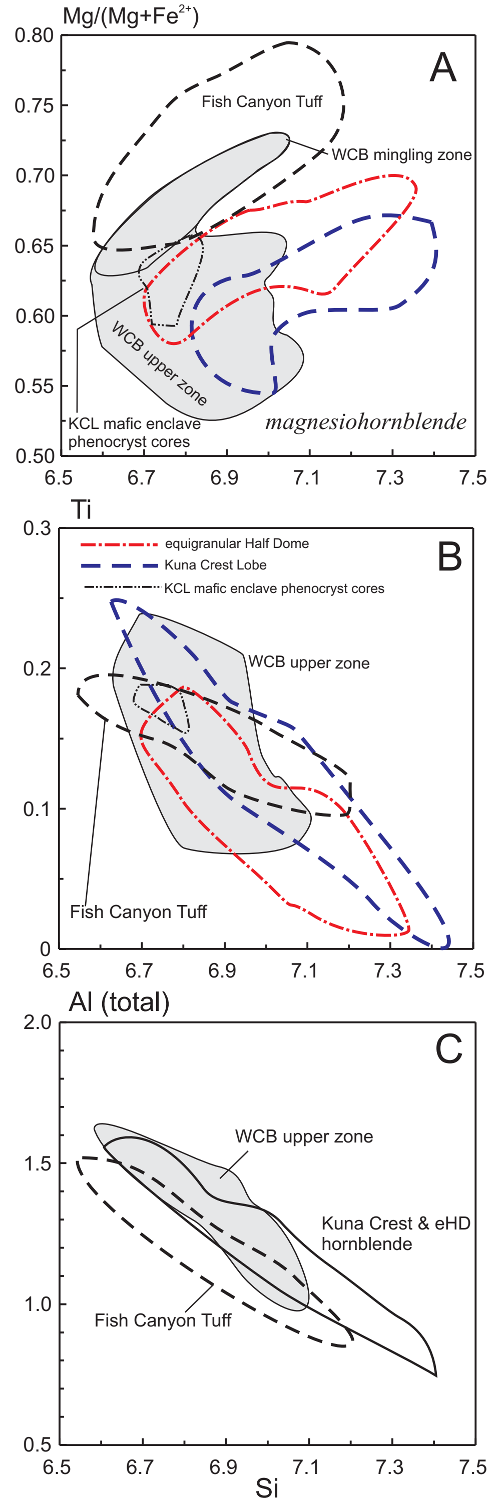

Figure 6.

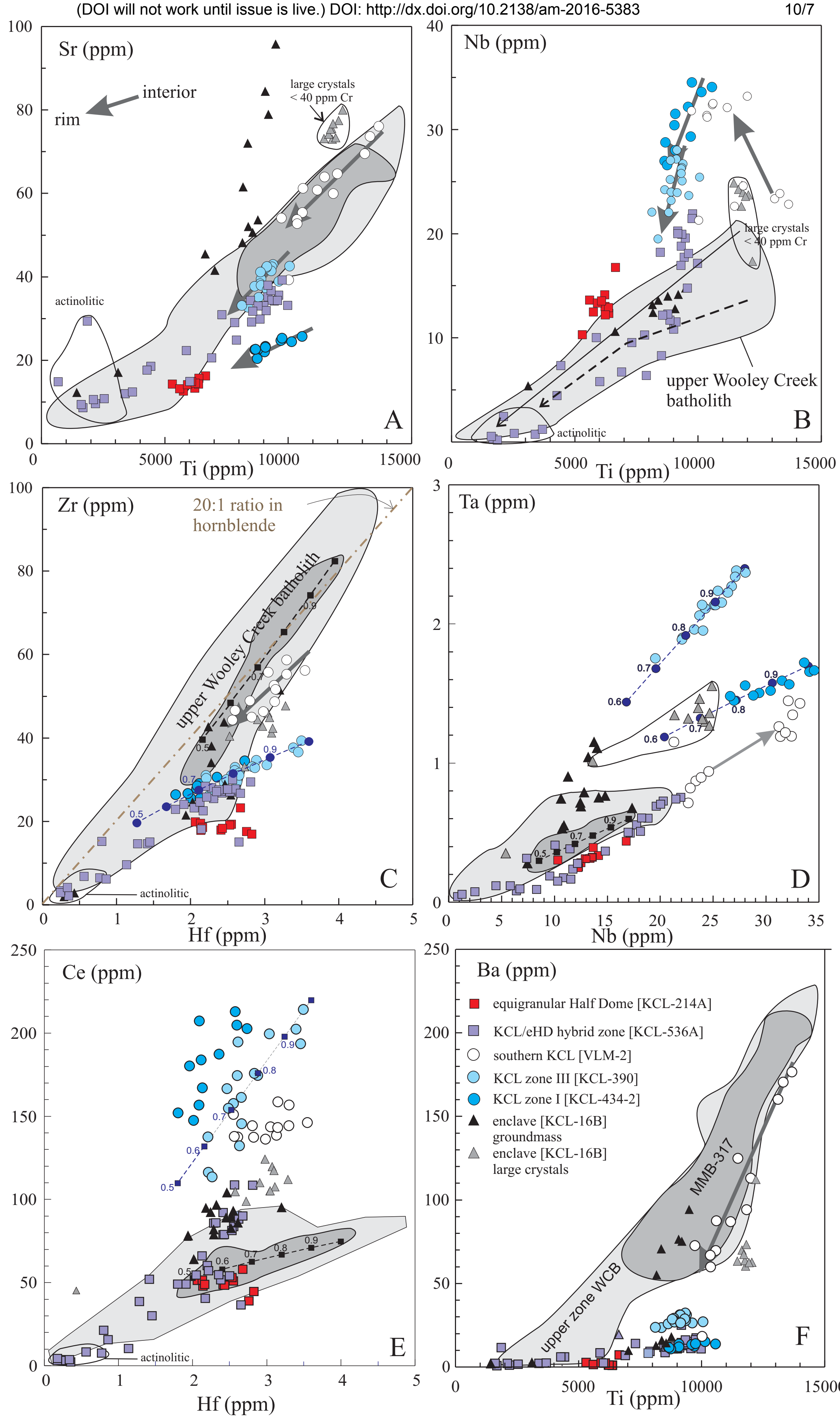
Sr (ppm)
interior
rim
large crystals
< 40 ppm Cr
actinolitic
A
Ti (ppm)
Nb (ppm)
large crystals
< 40 ppm Cr
upper Wooley Creek batholith
actinolitic
B
Ti (ppm)
Zr (ppm)
20:1 ratio in hornblende
upper Wooley Creek batholith
actinolitic
C
Hf (ppm)
Ta (ppm)
D
Nb (ppm)
Ce (ppm)
actinolitic
E
Hf (ppm)
Ba (ppm)
equigranular Half Dome [KCL-214A]
KCL/eHD hybrid zone [KCL-536A]
southern KCL [VLM-2]
KCL zone III [KCL-390]
KCL zone I [KCL-434-2]
enclave [KCL-16B] groundmass
enclave [KCL-16B] large crystals
MMB-317
upper zone WCB
F
Ti (ppm)

Figure 7

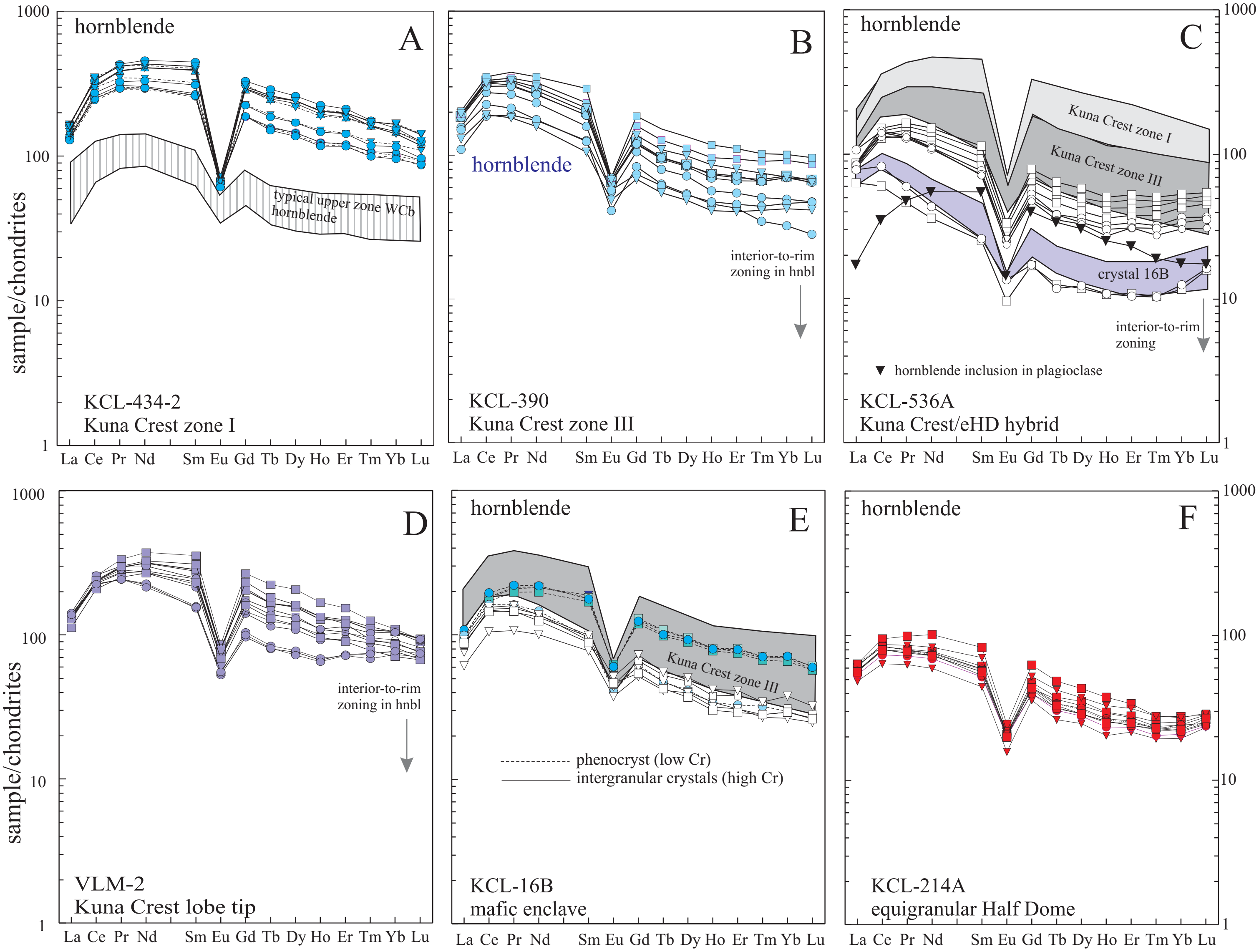
hornblende
A
typical upper zone WCb hornblende
KCL-434-2
Kuna Crest zone I
B
hornblende
interior-to-rim zoning in hnbl
KCL-390
Kuna Crest zone III
C
Kuna Crest zone I
Kuna Crest zone III
crystal 16B
interior-to-rim zoning
hornblende inclusion in plagioclase
KCL-536A
Kuna Crest/eHD hybrid
D
interior-to-rim zoning in hnbl
VLM-2
Kuna Crest lobe tip
E
Kuna Crest zone III
phenocryst (low Cr)
intergranular crystals (high Cr)
KCL-16B
mafic enclave
F
KCL-214A
equigranular Half Dome
sample/chondrites
1000
100
10
1
La Ce Pr Nd Sm Eu Gd Tb Dy Ho Er Tm Yb Lu

Figure 8